



The Abdus Salam
**International Centre
for Theoretical Physics**

Turbulent Fluid Flows in Definite Geometries and Numerical Solutions

Dr. Najmeh Foroozani

The Abdus Salam International Centre for Theoretical Physics (ICTP), Trieste Italy

nforooza@ictp.it

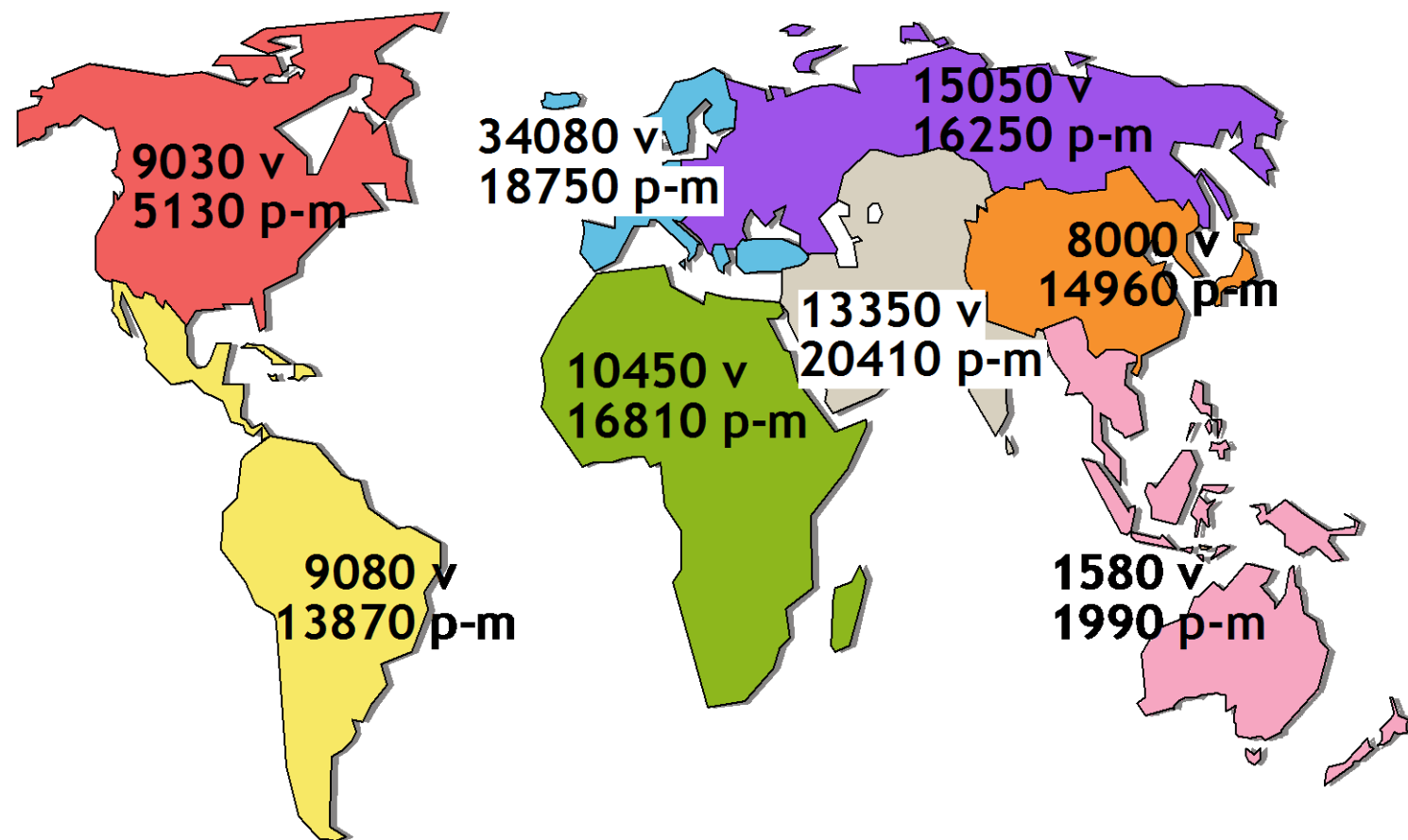
Complex Fluid Flows and Its Environmental Applications

University of Lagos, Nigeria

6th – 11th June 2016



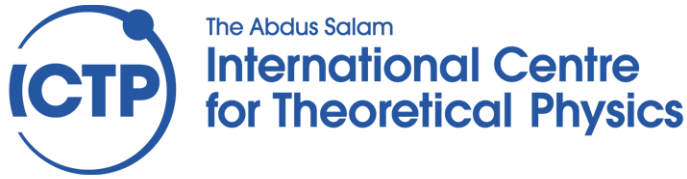
ICTP VISITORS STATISTICS, 1970-2006



area	visitors	p-m
North America	9030	5130
Latin America	9080	13870
Western Europe	34080	18750
Eastern Europe	15050	16250

area	visitors	p-m
Africa	10450	16810
Middle East and South Asia	13350	20410
South East Asia and the Pacific	1580	1990
Far East	8000	14960

v=visitors p-m=person-months



Programs at ICTP

**Diploma (ICTP),
Masters (with Italian partners)
Ph.D. (both Italian University system and IAEA SANDWICH).
Post-doctoral appointments
Scientific Associates
Training and research in Italian Laboratories Fellowships
Schools; Colleges; Workshops; Conferences
Electronic access to scientific literature
Support for regional conferences, often with other donors**

Recall

- Equations of motion for an incompressible flow:

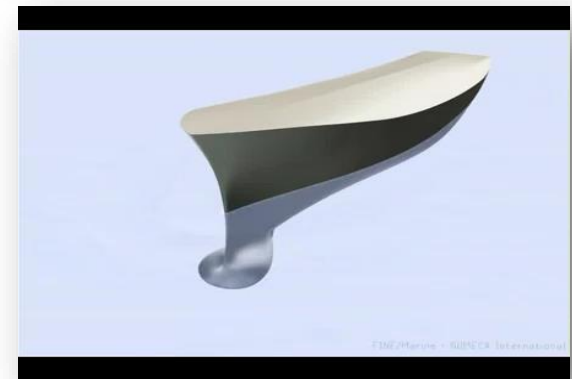
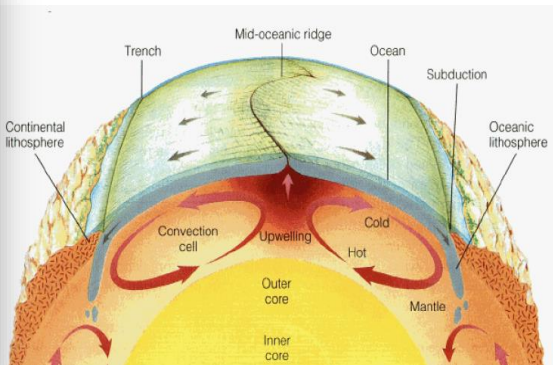
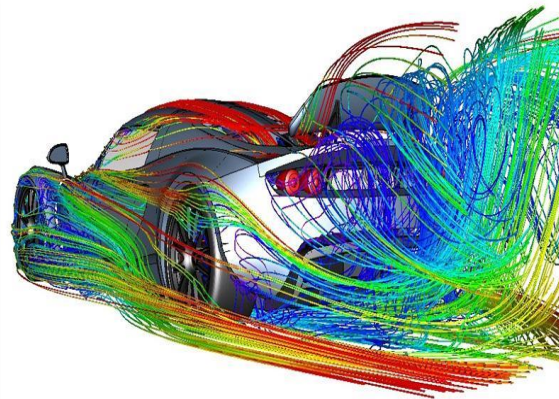
$$\frac{\partial u}{\partial x} + \frac{\partial v}{\partial y} + \frac{\partial w}{\partial z} = 0$$

$$\rho \left(\frac{\partial u}{\partial t} + u \frac{\partial u}{\partial x} + v \frac{\partial u}{\partial y} + w \frac{\partial u}{\partial z} \right) = - \frac{\partial P}{\partial x} + \rho g_x + \mu \left(\frac{\partial^2 u}{\partial x^2} + \frac{\partial^2 u}{\partial y^2} + \frac{\partial^2 u}{\partial z^2} \right)$$

$$\rho \left(\frac{\partial v}{\partial t} + u \frac{\partial v}{\partial x} + v \frac{\partial v}{\partial y} + w \frac{\partial v}{\partial z} \right) = - \frac{\partial P}{\partial y} + \rho g_y + \mu \left(\frac{\partial^2 v}{\partial x^2} + \frac{\partial^2 v}{\partial y^2} + \frac{\partial^2 v}{\partial z^2} \right)$$

$$\rho \left(\frac{\partial w}{\partial t} + u \frac{\partial w}{\partial x} + v \frac{\partial w}{\partial y} + w \frac{\partial w}{\partial z} \right) = - \frac{\partial P}{\partial z} + \rho g_z + \mu \left(\frac{\partial^2 w}{\partial x^2} + \frac{\partial^2 w}{\partial y^2} + \frac{\partial^2 w}{\partial z^2} \right)$$

Very few examples of CFD ...



CFD potentially provides an unlimited power for solving any flow problems

Recall

- Equations of motion for an incompressible flow:

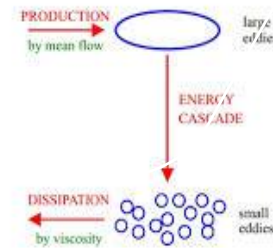
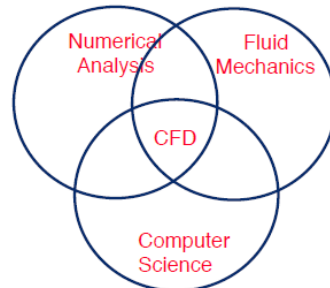
$$\frac{\partial u}{\partial x} + \frac{\partial v}{\partial y} + \frac{\partial w}{\partial z} = 0$$

$$\rho \left(\frac{\partial u}{\partial t} + u \frac{\partial u}{\partial x} + v \frac{\partial u}{\partial y} + w \frac{\partial u}{\partial z} \right) = - \frac{\partial P}{\partial x} + \rho g_x + \mu \left(\frac{\partial^2 u}{\partial x^2} + \frac{\partial^2 u}{\partial y^2} + \frac{\partial^2 u}{\partial z^2} \right)$$

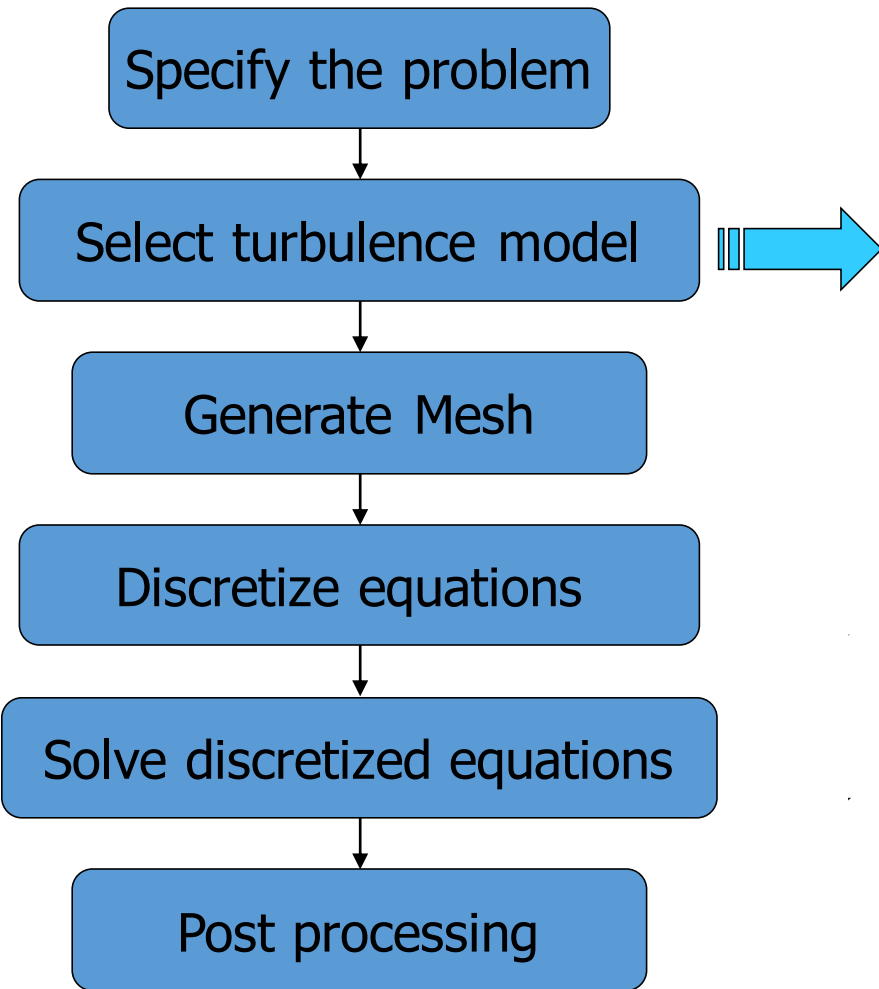
$$\rho \left(\frac{\partial v}{\partial t} + u \frac{\partial v}{\partial x} + v \frac{\partial v}{\partial y} + w \frac{\partial v}{\partial z} \right) = - \frac{\partial P}{\partial y} + \rho g_y + \mu \left(\frac{\partial^2 v}{\partial x^2} + \frac{\partial^2 v}{\partial y^2} + \frac{\partial^2 v}{\partial z^2} \right)$$

$$\rho \left(\frac{\partial w}{\partial t} + u \frac{\partial w}{\partial x} + v \frac{\partial w}{\partial y} + w \frac{\partial w}{\partial z} \right) = - \frac{\partial P}{\partial z} + \rho g_z + \mu \left(\frac{\partial^2 w}{\partial x^2} + \frac{\partial^2 w}{\partial y^2} + \frac{\partial^2 w}{\partial z^2} \right)$$

CFD Gives You Wings



CFD road map



Turbulence models

- These are semi-empirical mathematical models introduced to CFD to describe the turbulence in the flow

Main topics

- Three levels of CFD simulations
- Classification of turbulence models
- Examples of popular models
- Special considerations
- General remarks about turbulence modelling

Finite difference (FD)

Starting from the differential form of the equations

The computational domain is covered by a grid

At each grid point, the differential equations (partial derivatives) are approximated

Only used in structured grids and normally straightforward

Disadvantage: conservation is not always guaranteed

Disadvantage: Restricted to simple geometries.

Finite Volume (FV)

Starting from the integral form of the equations

The solution domain is covered by control volumes (CV)

The conservation equations are applied to each CV

The FV can accommodate any type of grid and suitable for complex geometries

The method is conservative (as long as surface integrals are the same for CVs sharing the boundary) *Most widely used method in CFD*

Disadvantage: more difficult to implement higher than 2nd order methods in 3D.

Finite element (FE)

The domain is broken into a set of discrete volumes: finite elements

The equations are multiplied by a weight function before they are integrated over the entire domain.

The solution is to search a set of non-linear algebraic equations for the computational domain.

Advantage: FE can easily deal with complex geometries.

Disadvantage: since unstructured in nature, the resultant matrices of linearized equations are difficult to find efficient solution methods. Not often used in CFD

Errors involved in CFD results

- Discretization errors
 - Depending on ‘schemes’ used. Use of higher order schemes will normally help to reduce such errors
 - Also depending on mesh size – reducing mesh size will normally help to reduce such errors. (skewness)
- Iteration errors
 - For converged solutions, such errors are relatively small.
- Turbulence modelling
 - Some turbulence models are proved to produce good results for certain flows
 - Some models are better than others under certain conditions
 - But no turbulence model can claim to work well for all flows
- Physical problem *vs* mathematical model
 - Approximation in boundary conditions
 - Use of a 2D model to simplify calculation
 - Simplification in the treatment of properties

Mean and fluctuating field

- A proper statistical description of turbulence takes advantage of the **Reynolds decomposition**. An instantaneous field can be decomposed into the:

mean field + fluctuating (zero-mean) field

Mean flow;

Time averaging

$$\bar{u}(\vec{x}) = \frac{1}{T} \int_t^{t+T} u(\vec{x}, t) dt$$

Space averaging

$$\left\{ \begin{array}{l} \bar{u}(t) = \frac{1}{V} \int_V u(\vec{x}, t) dV \\ \bar{u}(x_1, t) = \frac{1}{L_2 L_3} \int_{x_2 x_3} u(\vec{x}, t) dx_2 dx_3 \quad x_1 \perp S \\ \bar{u}(x_1, x_2, t) = \frac{1}{L_3} \int_{x_3} u(\vec{x}, t) dx_3 \quad x_1, x_2 \perp x_3 \end{array} \right.$$

Ensemble averaging

$$\bar{u}(\vec{x}, t) = \sum_{n=1}^M \bar{u}_n(\vec{x}, t)$$

We can write;

$$u(\vec{x}, t) = U(\vec{x}) + \textcolor{red}{u'(\vec{x}, t)}$$

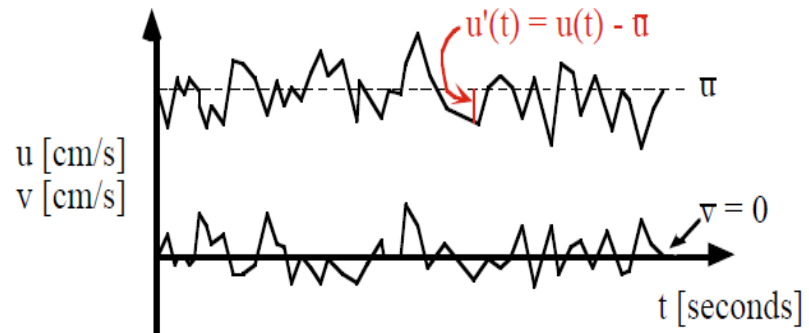
note : $U' = \frac{1}{T} \int_t^{t+T} u'(\vec{x}, t) dt = 0$

- Similar fluctuations for pressure, temperature, and species concentration values.

Turbulent Fluctuation:

$$u'(t) = u(t) - \bar{u} \quad : \text{continuous record}$$

$$u'_i = u_i - \bar{u} \quad : \text{discrete points}$$



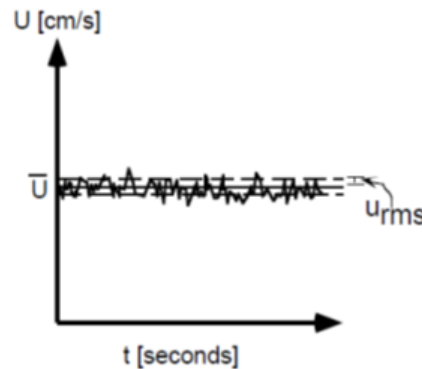
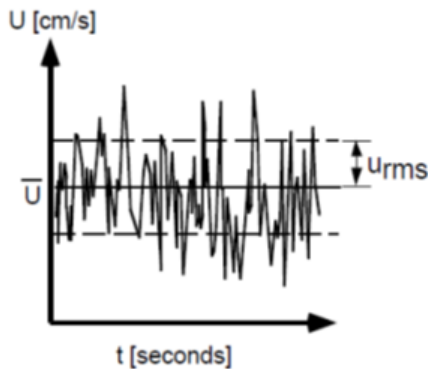
Turbulence Strength:

$$u_{rms} = \sqrt{\overline{u'(t)^2}} = \sqrt{\frac{1}{N} \sum_{i=1}^N (u'_i)^2}$$

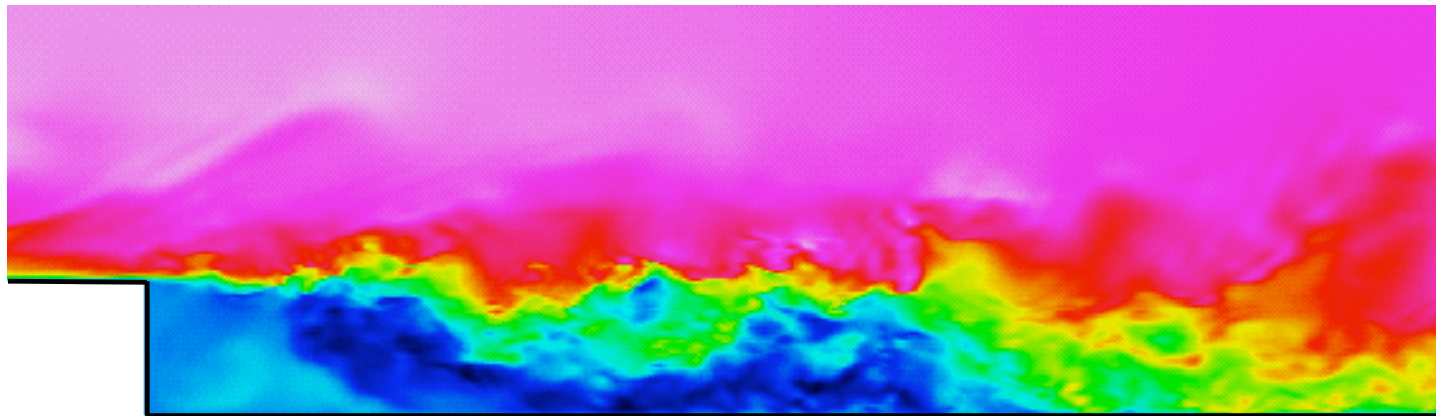
continuous record discrete, equi-spaced

Turbulence Intensity:

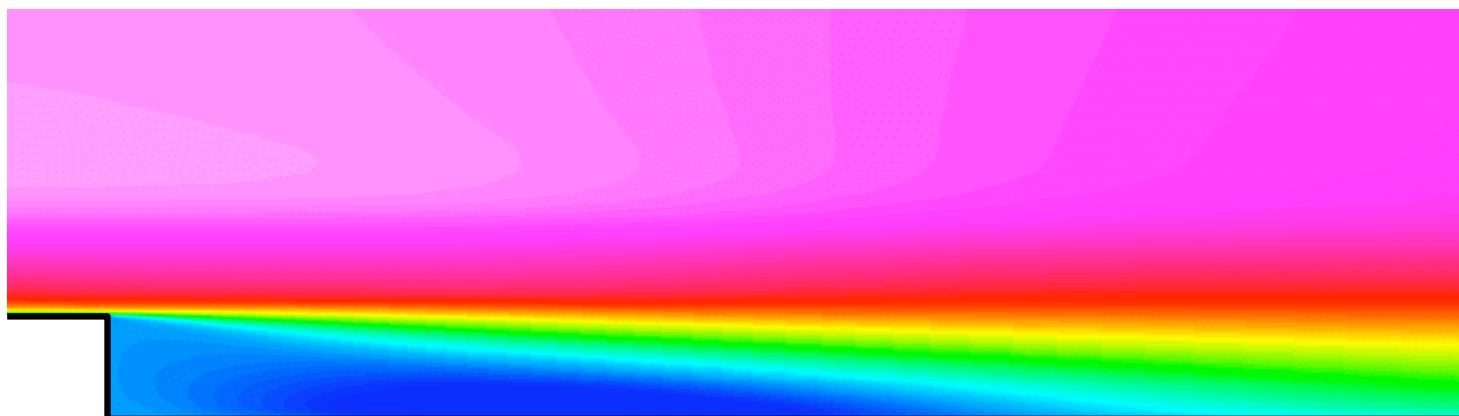
$$u_{rms}/\bar{u}$$



Instantaneous velocity contour

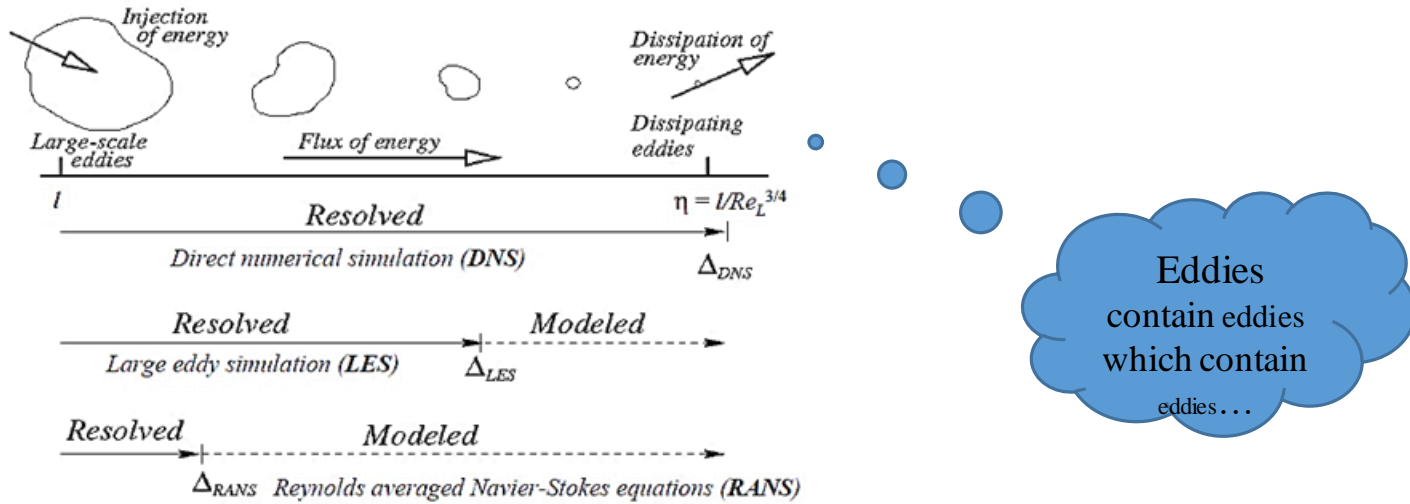


Time-averaged velocity contour



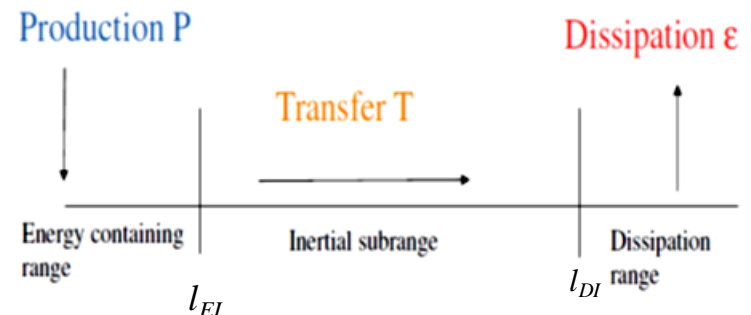
Energy Transfer/Turbulent scales

- The large eddies are unstable and break up, transferring their energy to somewhat smaller eddies.
- These smaller eddies undergo a similar break-up process and transfer their energy to yet smaller eddies.
- This energy cascade – in which energy is transferred to successively smaller and smaller eddies – continues until the Reynolds number $\text{Re}(l) \equiv u(l)l/\nu$ is sufficiently small that the eddy motion is stable, and molecular viscosity is effective in dissipating the kinetic energy.
- At these small scales, the kinetic energy of turbulence is converted into heat.



Kolmogorov
length scale

Dissipation ϵ



Kolmogorov's hypothesis of local isotropy states that *at sufficiently high Reynolds numbers, the small-scale turbulent motions are statistically isotropic*

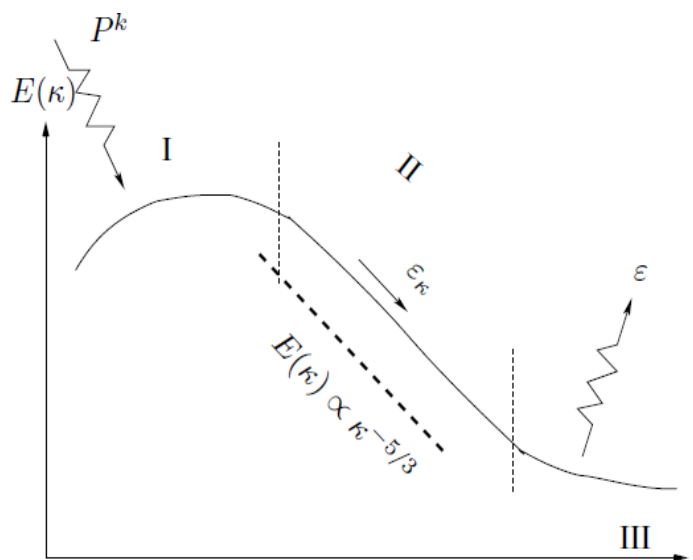
Here, the term local isotropy means isotropy at small scales. Large scale turbulence may still be anisotropic. l_{EI} is the length scale that forms the demarcation between the large scale anisotropic eddies ($l > l_{EI}$) and the small scale isotropic eddies ($l < l_{EI}$). For many high Reynolds number flows l_{EI} can be estimated as $l_{EI} \approx l_0/6$.

Energy Spectrum

Dimensional analysis gives:

$$E(\kappa) = C \epsilon^{2/3} \kappa^{-5/3}$$

This is the famous Kolmogorov “ $-5/3$ ” spectrum and C is the universal Kolmogorov constant, which experimentally was determined to be $C = 1.5$. (K. R. Sreenivasa (1995))

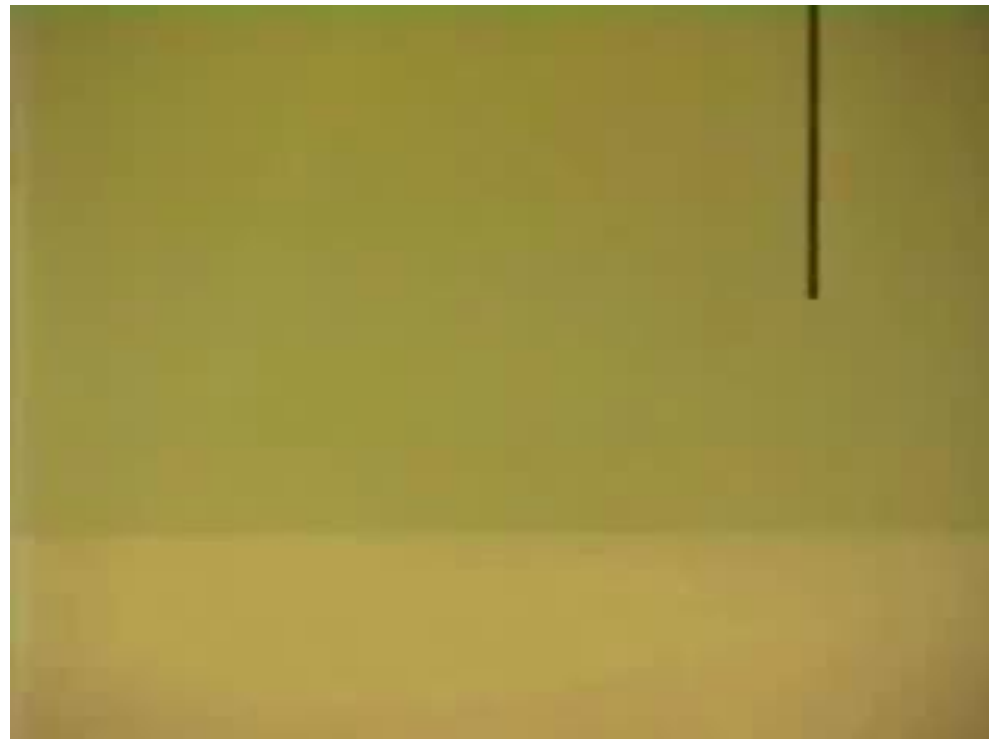


Spectrum for turbulent kinetic energy, κ . I: Range for the large, energy containing eddies. II: the inertial subrange. III: Range for small, isotropic scales

Some notes on boundary layers

**....perhaps the hardest place to use Bernoulli's equation
(so don't)**

Why viscosity is so important in fluid mechanics?

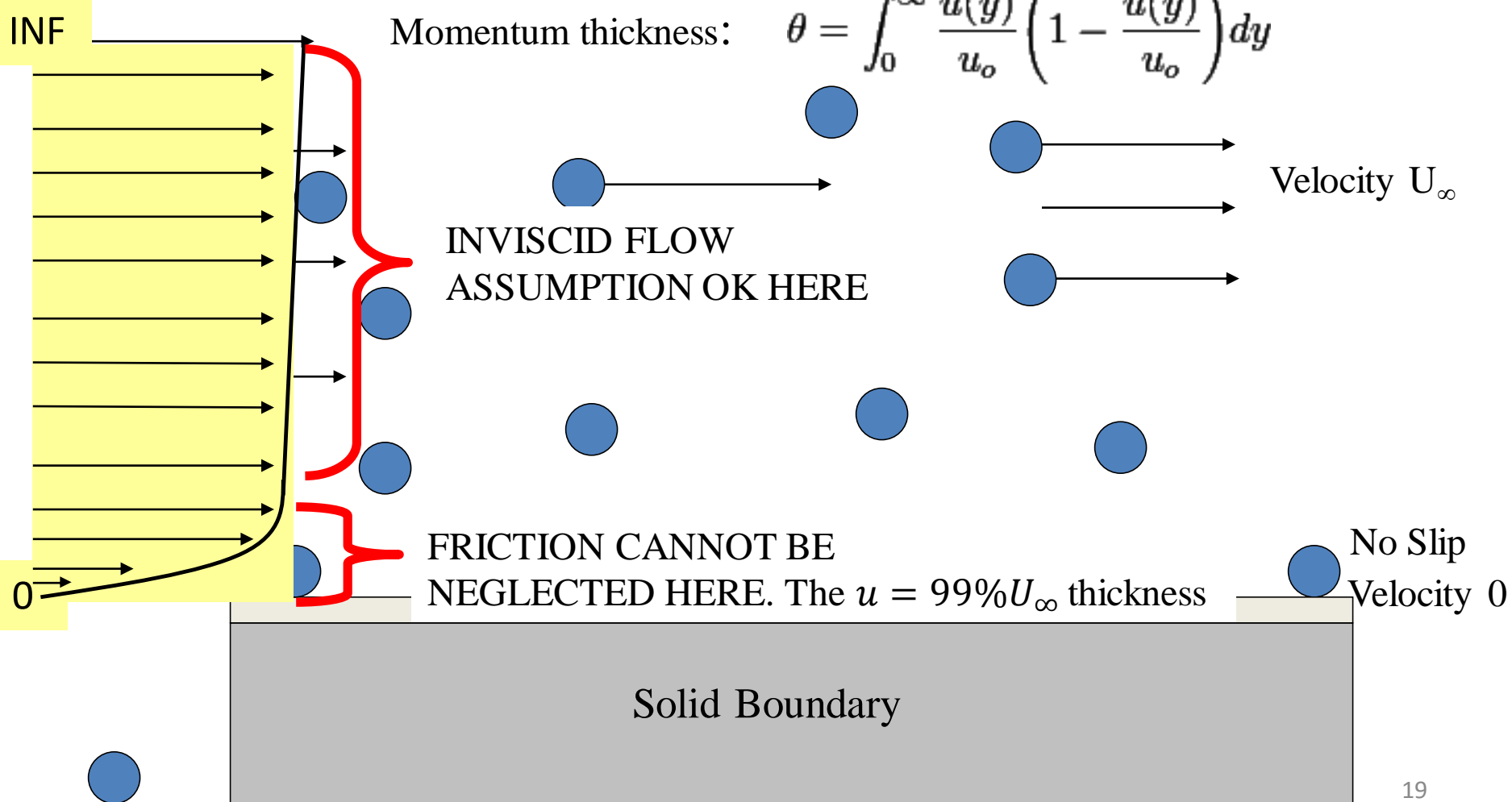


This so-called "**no-slip**" condition is a very important one that must be satisfied in any accurate analysis of fluid flow phenomena.

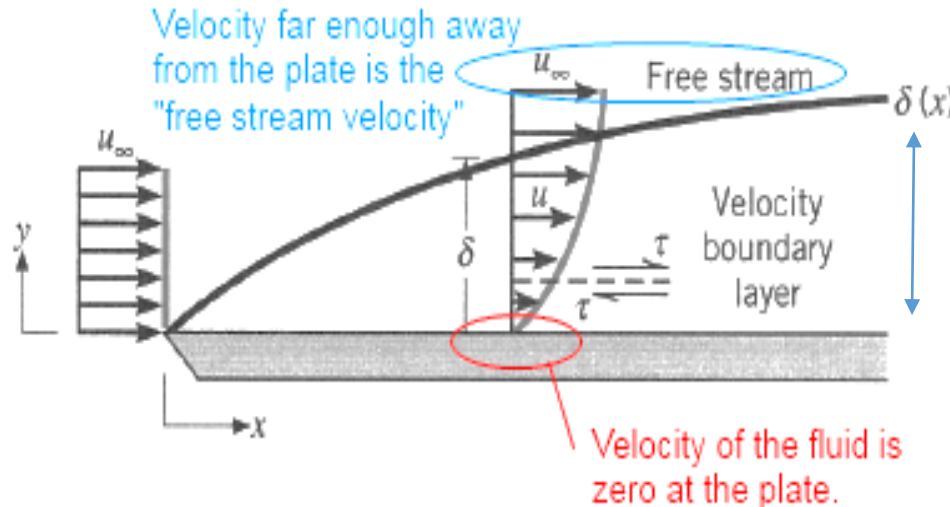
Boundary layer over flat plate

Displacement thickness $\delta^* = \int_0^\infty \left(1 - \frac{u(y)}{u_\infty}\right) dy$

Momentum thickness: $\theta = \int_0^\infty \frac{u(y)}{u_\infty} \left(1 - \frac{u(y)}{u_\infty}\right) dy$



Viscous boundary layer



- ❑ Most of the flow is unaffected by the presence of the plate. However, in the thin region closest to the wall, the velocity decreases to zero.

So divide the flow region around bodies into 2 zones:

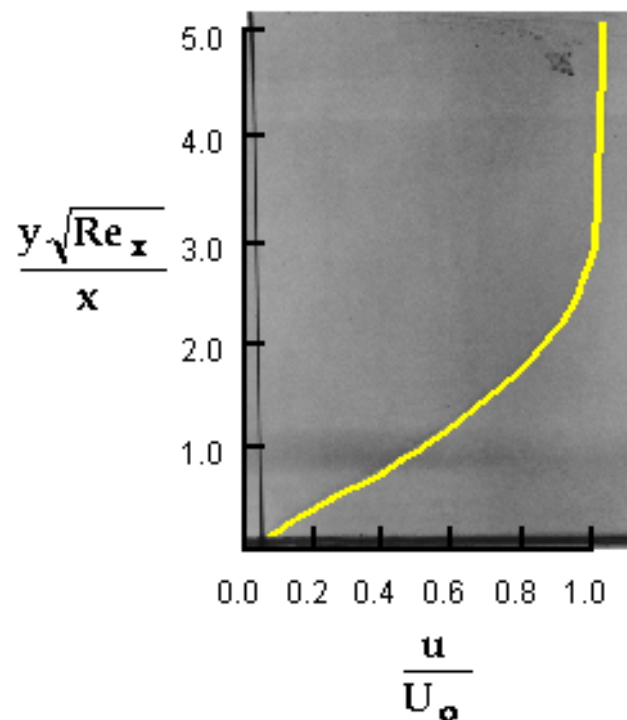
I) The near-wall region in which:

- ✓ The flow is rotational
- ✓ The Bernoulli's Equation fails
- ✓ Viscous effect is important

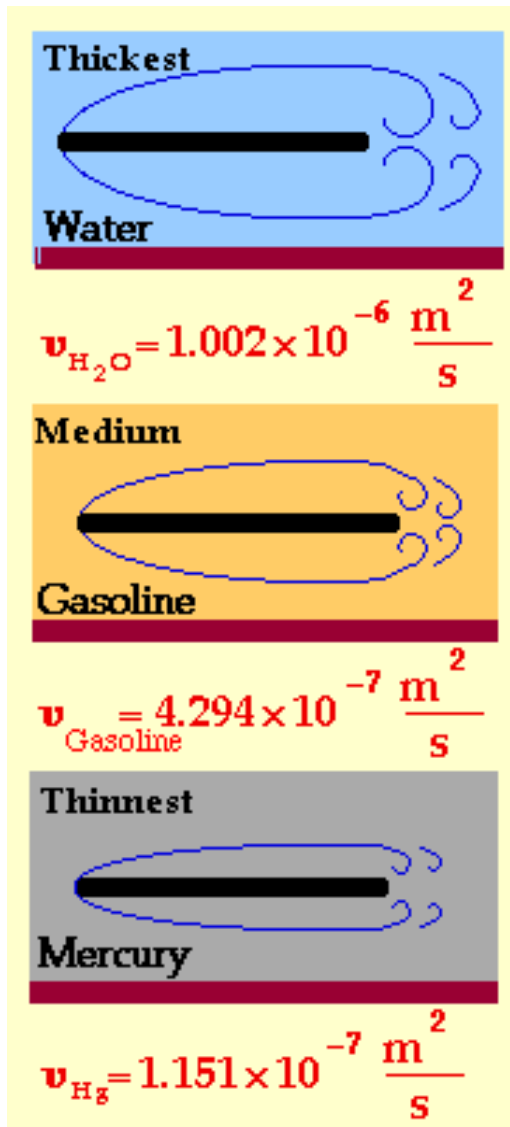
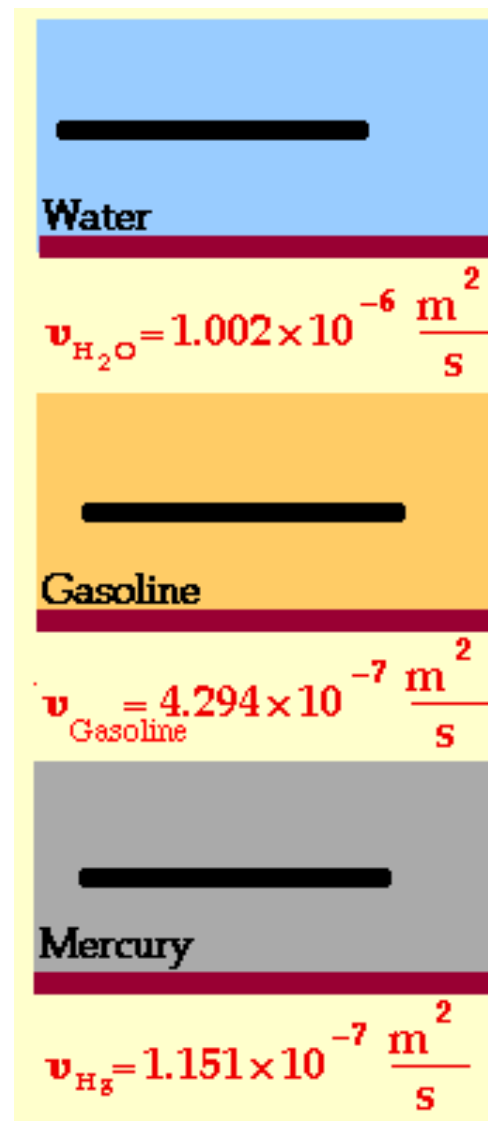
II) Flow region far from body in which:

- ✓ The flow is irrotational
- ✓ The Bernoulli Eq. holds
- ✓ Viscous effect is damped

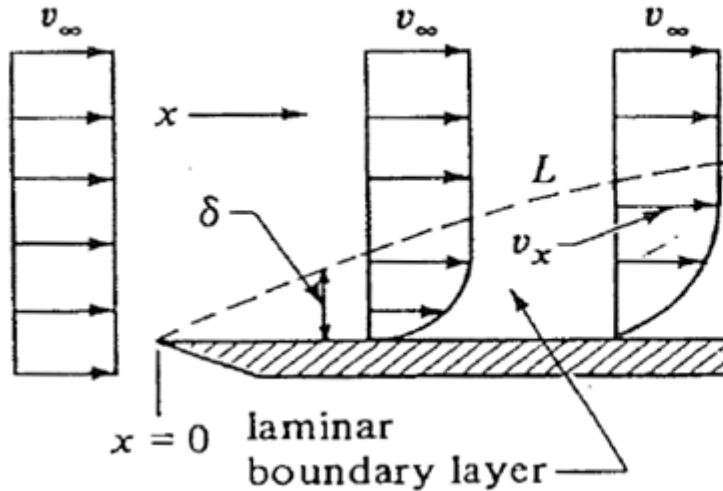
BL thicknesses and fluid properties



$$Re_x = \frac{\rho U_\infty x}{\mu} = \frac{U_\infty x}{\nu}$$



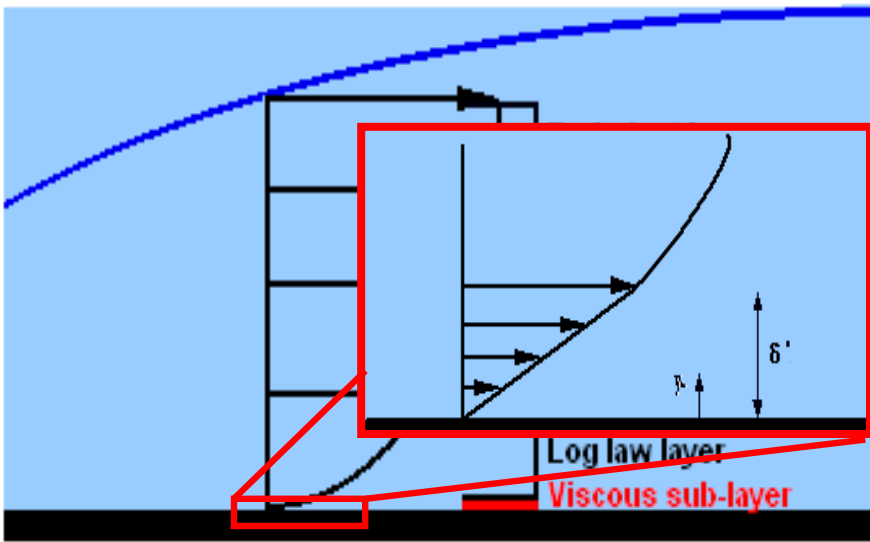
Turbulent boundary layer (TBL)



Turbulence near the wall

- For wall-bounded flows, turbulence initiates near the wall

The universal law of the wall



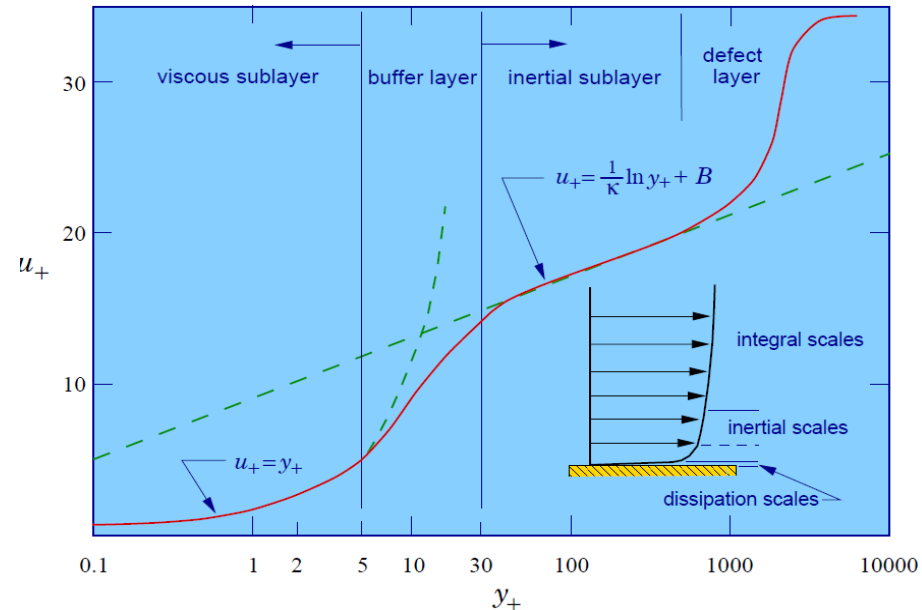
$$y^+ = \frac{yu_\tau}{\nu} \quad u^+ = \frac{u}{u_\tau} \quad \text{where}$$

$$u_\tau = \sqrt{\frac{\tau_{wall}}{\rho}}$$

u^+ : local velocity

u_τ : friction velocity

τ_{wall} : wall shear stress

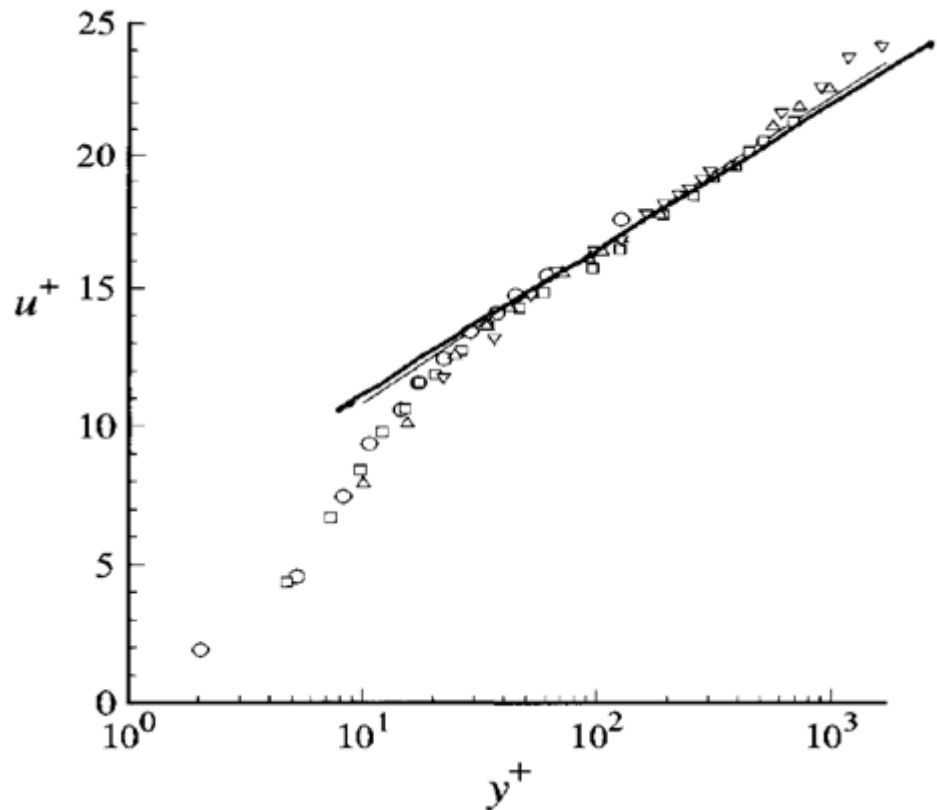


Dimensionless velocity profiles plotted in the near-wall coordinates. The linear section in the semi-log plot is called the **universal law of the wall layer**, or log law layer, for equilibrium turbulent boundary layers (TBL).

This figure shows measured profiles of $u^+(y^+)$ for turbulent channel flow at Reynolds numbers between $Re_0 \approx 3,000$ and $Re_0 \approx 40,000$. It may be seen that the data collapse to a single curve – in confirmation of the law of the wall – and that for $y^+ > 30$ the data conform to the log law, except near the channel's mid plane (last few data points for each Reynolds number)

The region between the viscous sublayer ($y^+ < 5$) and the log low region ($y^+ > 30$) is called the buffer layer. It is the transition region between the viscosity dominated and the turbulence dominated parts of the flow.

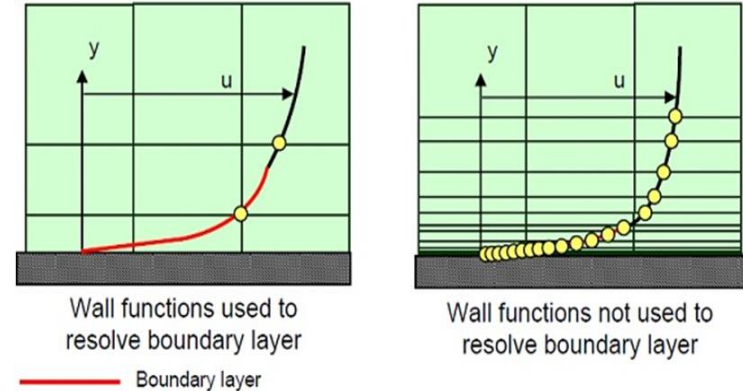
S. B. Pope, page 274



Mean velocity profiles in fully developed turbulent channel flow measured by Wei and Willmarth (1989): \circ , $Re_0 = 2,970$; \square , $Re_0 = 14,914$; Δ , $Re_0 = 22,776$; ∇ , $Re_0 = 39,582$; line, the log law

How to deal with it in CFD

- In the near-wall region, the turbulent boundary layer is very thin and the solution gradients are very high, but accurate calculations in the near-wall region are paramount to the success of the simulation
- We can use a very fine mesh to resolve this region, but it is very costly for industrial CFD applications



- For equilibrium turbulent boundary layers, the Universal Law of the Wall (or “log law”) can be used in order to alleviate the problem:
 - Velocity profile and wall shear stress obtained from the log law are used to set the boundary values of stresses for the wall-adjacent cells.
 - The equilibrium assumption is used to set boundary conditions for turbulent kinetic energy (k), dissipation rate (ε) or specific dissipation rate (ω).
 - Non-equilibrium wall function method attempts to improve the results for flows with higher pressure gradients, separations, reattachment and stagnation
 - Similar log-laws are also constructed for the energy and species equations
 - Benefit: Wall functions allow the use of a relatively coarse mesh in the near-wall region thereby reduce the computational cost.

If you are interested in CFD now !

www.cfdonline.com

www.ictp.it

www.units.it



Turbulent Fluid Flows in Definite Geometries and Numerical Solutions

Dr. Najmeh Foroozani

Dr. Abiala & Dr. Akinnukawe

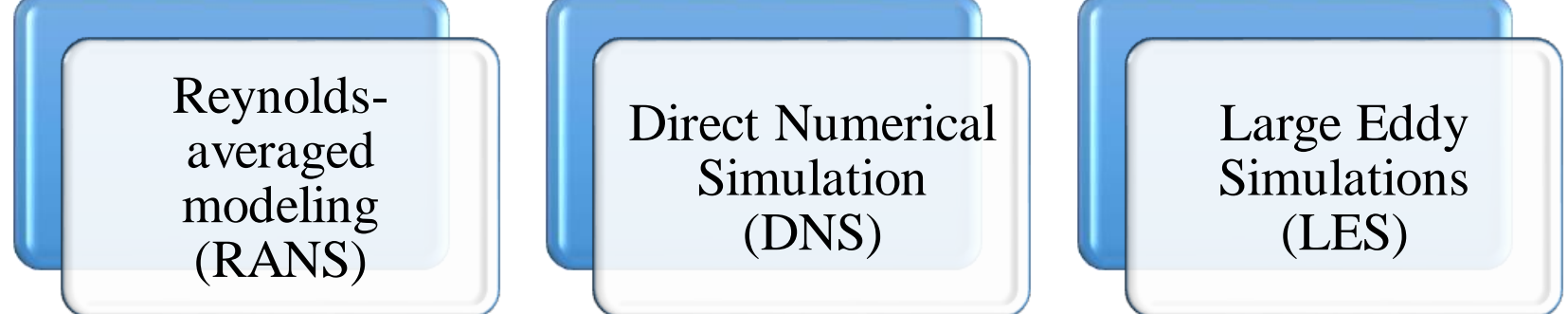
Complex Fluid Flows and Its Environmental Applications

University of Lagos, Nigeria

6th – 11th June 2016

An introduction to modeling and simulations

The three level of simulations



Reynolds-Averaged NS equations (RANS)

A more sophisticated method involves the use of Reynolds averaging: the long term average of a quantity f is defined as

$$\bar{f} = \frac{1}{T} \int_t^{t+T} f(\tau) d\tau$$

where T is a time interval much longer than all the time scales of the turbulent flow.

By averaging the Navier-Stokes equations, we obtain the Reynolds averaged Navier-Stokes (RANS) equations;

$$\frac{\partial u_i}{\partial x_i} = 0, \quad \rho \frac{\partial u_i}{\partial t} + \rho \frac{\partial}{\partial x_j} (u_j u_i) = - \frac{\partial p}{\partial x_i} + \frac{\partial}{\partial x_j} (2\mu S_{ij})$$

Decompose pressure and velocity into mean part and fluctuating part $u_i = \bar{u} + u'$

$$\frac{\partial \bar{u}_i}{\partial x_i} = 0, \quad \rho \frac{\partial \bar{u}_i}{\partial t} + \rho \frac{\partial}{\partial x_j} (\bar{u}_j \bar{u}_i) = - \frac{\partial \bar{p}}{\partial x_i} + \frac{\partial}{\partial x_j} (2\mu S_{ij} - \underbrace{\rho \bar{u}'_i \bar{u}'_j}_{\text{Reynolds stress tensor } R_{ij}})$$

$$R_{ij} = -\rho \begin{bmatrix} \overline{u'u'} & \overline{u'v'} & \overline{u'w'} \\ \overline{v'u'} & \overline{v'v'} & \overline{v'w'} \\ \overline{w'u'} & \overline{w'v'} & \overline{w'w'} \end{bmatrix}$$

Reynolds stress
tensor R_{ij}

In order to close the RANS equations, the Reynolds stress tensor must be modeled.

How can we close the RANS equations?

I) Eddy viscosity model (stress is proportional to the stress)

- We express the elements of the Reynolds stress tensor through the mean shear introducing the concept of eddy viscosity

$$\overline{u'_i u'_j} = -2\nu_t S_{ij} = -\nu_t \left(\frac{\partial U_i}{\partial x_j} + \frac{\partial U_j}{\partial x_i} \right)$$

And we find ν_t by means of **turbulence models**

Note:

- 1) ν_t is a characteristic of the FLOW field, not of the fluid! Unlike an isothermal laminar flow in which viscosity is a constant which varies with position throughout the flow field
- 2) It is a statistical quantities, so it varies along the non-homogeneous directions.

II) Reynolds stress model

The model is more complex since there are more equations to solve, and computationally expensive than I

Direct Numerical Simulation (DNS)

- A **direct numerical simulation (DNS)** is a simulation in CFD in which the NS-equations are numerically solved **without any** turbulence model. This means that the whole range of spatial and temporal scales of the turbulence must be resolved. All the spatial scales of the turbulence must be resolved in the computational mesh, from the smallest dissipative scales (Kolmogorov microscales), up to the integral scale L , associated with the motions containing most of the kinetic energy.
- ◆ Given the current processing speed and memory of the largest computers, only very modest Reynolds number flows with simple geometries are possible. i.e., The cost of a simulation increases as Re^3
- ◆ **Advantages:** DNS can be used as **numerical flow visualization** and can provide more information than experimental measurements; DNS can be used to understand the mechanisms of turbulent production and dissipation.
- ◆ **Disadvantages:** Requires supercomputers; limited to simple geometries.
- ◆ **Is DNS a useful tool?**

Large Eddy Simulation (LES)

- KEY IDEA is to directly **solve** the unsteady and 3D large-scale energy-carrying structures and to **parametrize** the more isotropic and dissipative small structures (subgrid-scales, SGS)
- Separation of the scales: application of a low-pass **filter** to the NS equations

$$\bar{f}(x) = \int_D f(x') G(x, x') dx'$$

$G(x, x')$ is the filter function

FIRST NEED TO SEPARATE THE FLOW FIELD

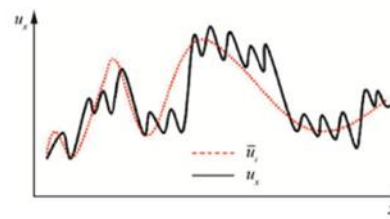


Large eddies, most energy and fluxes,
explicitly calculated, must be resolved.



Small eddies, little energy and fluxes,
parameterized

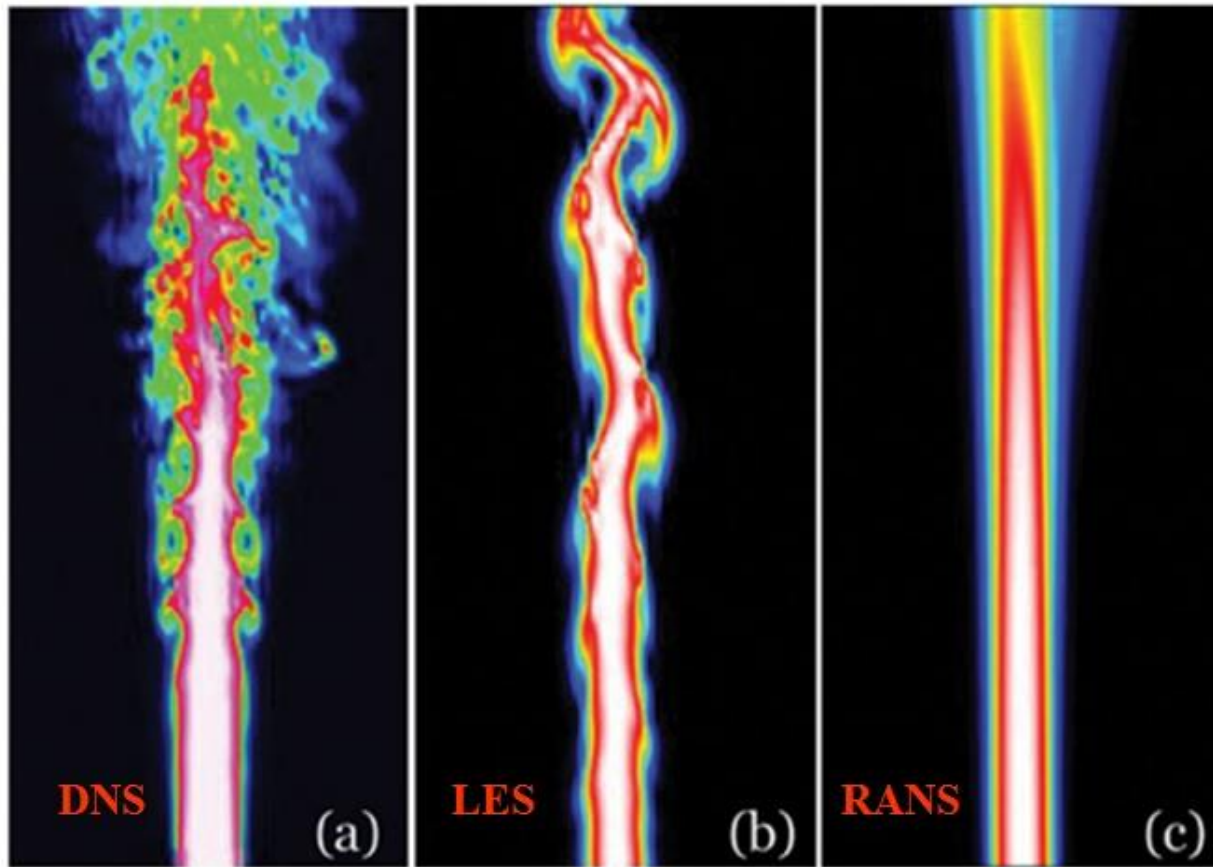
- LES is a three dimensional, time dependent and computationally expensive simulation, though less expensive than DNS.



LES vs RANS

- LES **can** handle many flows which RANS (Reynolds Averaged Navier Stokes) **cannot**; the reason is that in LES more, turbulent scales are resolved. Here are some examples that could be studied by LES only:
 - Flows with large separation
 - Bluff-body flows (e.g. flow around a car); the wake often includes large, unsteady, turbulent structures
 - Transition
 - In RANS all turbulent scales are modeled \Rightarrow inaccurate
 - In LES only small, isotropic turbulent scales are modeled \Rightarrow accurate
 - LES is *very* much more expensive than RANS.

DNS, LES and RANS

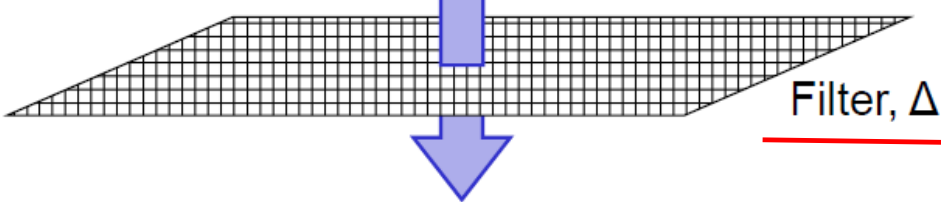


DNS (left), LES (middle) and RANS (right) predictions of a turbulent jet. LES requires less computational effort than DNS, while delivering more detail than the inexpensive RANS. (A. Maries, University of Pittsburgh)

LES

$$u_i(\mathbf{x}, t) = \bar{u}_i(\mathbf{x}, t) + u'_i(\mathbf{x}, t)$$

↑ Instantaneous component ↑ Resolved Scale ↑ Subgrid Scale

$$\frac{\partial u_i}{\partial t} + \frac{\partial (u_i u_j)}{\partial x_j} = -\frac{1}{\rho} \frac{\partial p}{\partial x_i} + \frac{\partial}{\partial x_j} \left(\nu \frac{\partial u_i}{\partial x_j} \right)$$


Filtered N-S equation

$$\frac{\partial \bar{u}_i}{\partial t} + \frac{\partial (\bar{u}_i \bar{u}_j)}{\partial x_j} = -\frac{1}{\rho} \frac{\partial \bar{p}}{\partial x_i} + \frac{\partial}{\partial x_j} \left(\nu \frac{\partial \bar{u}_i}{\partial x_j} \right) - \frac{\partial \tau_{ij}}{\partial x_j}$$

$$\tau_{ij} = \rho (\bar{u}_i u_j - \bar{u}_i \bar{u}_j)$$

(Subgrid scale Turbulent stress)

- Spectrum of turbulent eddies in the Navier-Stokes equations is filtered:
 - The filter is a function of grid size
 - Eddies smaller than the grid size are removed and modeled by a subgrid scale (SGS) model.
 - Larger eddies are directly solved numerically by the filtered transient NS equation

Filtered momentum equation

- Filter the momentum eq. with an arbitrary homogenous filter of width $\bar{\Delta}$ homogeneity of filter allows commutation with differentiation:

$$\frac{\partial \bar{u}_i}{\partial t} + \frac{\partial (\bar{u}_i \bar{u}_j)}{\partial x_j} = - \frac{\partial \bar{p}}{\partial x_i} + \frac{1}{\text{Re}} \frac{\partial^2 \bar{u}_i}{\partial x_j^2}$$

- $\bar{u}_i \bar{u}_j = \bar{u}_i \bar{u}_j + \bar{u}_i \bar{u}_j - \bar{u}_i \bar{u}_j$ leads to

$$\frac{\partial \bar{u}_i}{\partial t} + \frac{\partial (\bar{u}_i \bar{u}_j)}{\partial x_j} = - \frac{\partial \bar{p}}{\partial x_i} + \frac{1}{\text{Re}} \frac{\partial^2 \bar{u}_i}{\partial x_j^2} - \frac{\partial \tau_{ij}}{\partial x_j}$$

$$\tau_{ij} = \bar{u}_i \bar{u}_j - \bar{u}_i \bar{u}_j$$

- τ_{ij} is an **unknown** stress accounting for the effect of the filtered-out small scales on the large scales governed by the filtered equation

Residual (subgrid-scale (SGS)) stress

- Note that in general: $A_{ij}^d \equiv A_{ij} - (1/3)\delta_{ij}A_{kk}$

Decompose the SGS stress as $\tau_{ij} = \tau_{ij}^d + \tau_{ij}^{iso}$

$$\tau_{ij}^d = (\underbrace{\bar{u}_i u_j - \bar{u}_i \bar{u}_j}_{\tau_{ij}}) - \frac{1}{3} \delta_{ij} (\underbrace{\bar{u}_k u_k - \bar{u}_k \bar{u}_k}_{\tau_{kk}})$$

↑
deviatoric (trace-free) component

$$\tau_{ij}^{iso} = \frac{1}{3} \delta_{ij} (\underbrace{\bar{u}_k u_k - \bar{u}_k \bar{u}_k}_{\tau_{kk}})$$

↑
isotropic component

- This decomposition leads to

$$\frac{\partial \bar{u}_i}{\partial t} + \frac{\partial(\bar{u}_i \bar{u}_j)}{\partial x_j} = -\frac{\partial \bar{P}}{\partial x_i} + \frac{1}{Re} \frac{\partial^2 \bar{u}_i}{\partial x_j^2} - \frac{\partial \tau_{ij}^d}{\partial x_j}$$

- The modified filtered pressure contains the isotropic part of the SGS stress

Filtered equations

$$\frac{\partial \bar{u}_i}{\partial x_i} = 0$$

SGS stress
↓

$$\frac{\partial \bar{u}_i}{\partial t} + \bar{u}_j \frac{\partial \bar{u}_i}{\partial x_j} = - \frac{\partial \bar{P}}{\partial x_i} + \frac{1}{\text{Re}} \frac{\partial^2 \bar{u}_i}{\partial x_j^2} - \frac{\partial \tau_{ij}^d}{\partial x_j} + Ri(\bar{\rho} - \bar{\rho}_b)$$

$$\frac{\partial \bar{\rho}}{\partial t} + \bar{u}_i \frac{\partial \bar{\rho}}{\partial x_i} = \kappa \frac{\partial^2 \bar{\rho}}{\partial x_i^2} - \frac{\partial \lambda_i}{\partial x_i} \leftarrow \text{SGS density flux}$$

SGS stress: $\tau_{ij}^d = (\bar{u}_i \bar{u}_j - \bar{u}_i \bar{u}_j)^d \equiv (\bar{u}_i \bar{u}_j - \bar{u}_i \bar{u}_j) - \frac{1}{3} \delta_{ij} (\bar{u}_k \bar{u}_k - \bar{u}_k \bar{u}_k)$

SGS density flux: $\lambda_i \equiv \overline{\rho u_i} - \bar{\rho} \bar{u}_i$ (obtained in same way as the SGS stress)

Comments on the filtered equations

- The filtered equations are numerically solved for the filtered $(\bar{u}_i, \bar{\rho}, \bar{P})$ variables describing the large scales
- The SGS stress and SGS density flux present closure problems and must be modeled or approximated in terms of filtered variables only
- In theory, the filter used to obtain the filtered equations is arbitrary
- In practice, the filter is inherently assumed by the discretization (i.e. the numerical method used to solve the filtered equations and the SGS models)
- The discretization can only represent (resolve) down to scales on the order of 1,2, or 3 times the grid cell size, h , thereby “filtering-out” smaller scales.

$$\bar{\Delta} = O(1h - 3h)$$

Smagorinsky SGS model

- Recall that the SGS stress and density buoyancy flux must be modeled or approximated

Smagorinsky (1967) model:

$$\tau_{ij}^d \equiv (\overline{u_i u_j} - \bar{u}_i \bar{u}_j)^d \approx -2\nu_T \bar{S}_{ij}$$

Both are trace-free

$$\nu_T = (C_S \bar{\Delta})^2 |\bar{S}| \quad | \bar{S} | = \sqrt{2 \bar{S}_{ij} \bar{S}_{ij}} \quad \bar{S}_{ij} = \frac{1}{2} \left(\frac{\partial \bar{u}_i}{\partial x_j} + \frac{\partial \bar{u}_j}{\partial x_i} \right)$$

Smagorinsky coefficient

Analogously: $\lambda_i \equiv \overline{\rho u_i} - \bar{\rho} \bar{u}_i \approx -\kappa_T (\partial \bar{\rho} / \partial x_i)$

$$\kappa_T = (C_\rho \bar{\Delta})^2 |\bar{S}|$$

The eddy (turbulent) viscosity

The turbulent viscosity has units L^2 / T . Because we are working with the smallest resolved scales, we can set $L = \bar{\Delta}$

- And we may have $T = (\bar{\Delta}^2 / \varepsilon)^{1/3} \Rightarrow \nu_T = C\varepsilon^{1/3}\bar{\Delta}^{4/3}$
- In a global sense, the rate of energy transfer within the inertial range is roughly equal to the SGS dissipation. Here we assume it locally:



$$\varepsilon \approx -\overbrace{\tau_{ij}^d \bar{S}_{ij}} = \nu_T |\bar{S}|^2 \Rightarrow \nu_T = \underbrace{C^{3/2} \bar{\Delta}^2} C_s^2 |\bar{S}|$$

Difficulties with the Smagorinsky model

Smagorinsky model:

$$\tau_{ij}^d \equiv (\overline{u_i u_j} - \bar{u}_i \bar{u}_j)^d \approx -2\nu_T \bar{S}_{ij}$$
$$\nu_T = (C_S \bar{\Delta})^2 |\bar{S}|$$

- For isotropic turbulence, Lilly (1967) showed that $C_S = 0.16$

Major difficulty:

- The constant coefficient allows for a non-vanishing turbulent viscosity at boundaries and in the presence of relaminarization
- The Smagorinsky coefficient should be a function of **space and time**
- In 1991, Germano and collaborators derived a dynamic expression for the Smagorinsky coefficient

Dynamic Smagorinsky model

- Recall filtering the N-S equations with an homogeneous filter of width

$$\frac{\partial \bar{u}_i}{\partial t} + \bar{u}_j \frac{\partial \bar{u}_i}{\partial x_j} = -\frac{\partial \bar{P}}{\partial x_i} + \frac{1}{\text{Re}} \frac{\partial^2 \bar{u}_i}{\partial x_j^2} - \frac{\partial \tau_{ij}^d}{\partial x_j} \quad \tau_{ij}^d \equiv (\bar{u}_i \bar{u}_j - \bar{u}_i \bar{u}_j)^d \approx -2(C_S \bar{\Delta})^2 |\bar{S}| \bar{S}_{ij}$$

Consider a new filter made up from successive applications of the 1st filter (above) and a new “**test**” filter. This “double” filter has width $\hat{\Delta}$

Application of this “double” filter is denoted by a “bar-hat” in the form of \hat{f}

With this new filter, the filtered momentum equation becomes:

$$\frac{\partial \hat{\bar{u}}_i}{\partial t} + \hat{\bar{u}}_j \frac{\partial \hat{\bar{u}}_i}{\partial x_j} = -\frac{\partial \hat{\bar{P}}}{\partial x_i} + \frac{1}{\text{Re}} \frac{\partial^2 \hat{\bar{u}}_i}{\partial x_j^2} - \frac{\partial T_{ij}^d}{\partial x_j} \quad T_{ij}^d \equiv (\bar{u}_i \bar{u}_j - \hat{\bar{u}}_i \hat{\bar{u}}_j)^d \approx -2(C'_S \hat{\Delta})^2 |\hat{S}| \hat{S}_{ij}$$

- **Scale invariance:** Both $\hat{\Delta}$ and $\bar{\Delta}$ are in the inertial range, thus $C'_S = C_S$

Dynamic Smagorinsky model

- Consider the following tensor proposed by Germano (GI) : $L_{ij}^d \equiv T_{ij}^d - \tau_{ij}^d$

$$L_{ij}^d = (\widehat{\overline{u_i u_j}} - \widehat{\bar{u}_i \bar{u}_j})^d - (\widehat{\overline{u_i u_j}} - \widehat{\bar{u}_i \bar{u}_j})^d = (\widehat{\overline{u_i u_j}} - \widehat{\bar{u}_i \bar{u}_j})^d \quad \leftarrow \text{(resolved)}$$

$$L_{ij}^d = -2(C_S \widehat{\Delta})^2 | \widehat{\bar{S}} | \widehat{\bar{S}_{ij}} + 2(C_S \overline{\Delta})^2 | \overline{\bar{S}} | \widehat{\bar{S}_{ij}} \quad \leftarrow \text{(modeled)}$$

- Minimization of the difference between these two with respect to C_S leads to:

$$(C_S \overline{\Delta})^2 = \frac{< L_{ij} M_{ij} >}{< 2M_{kl} M_{kl} >}$$

$$M_{ij} = | \bar{S} | \widehat{\bar{S}_{ij}} - \alpha | \widehat{\bar{S}} | \widehat{\bar{S}_{ij}}$$

$< \cdot >$ - Averaging in statistically homogenous direction(s)

$$L_{ij} = \widehat{\overline{u_i u_j}} - \widehat{\bar{u}_i \bar{u}_j} \quad \alpha = \left(\frac{\widehat{\Delta}}{\overline{\Delta}} \right)^2$$

- Explicit application of test filter (denoted by a “hat”) is required, unlike 1st filter

LES methodology used in computations

$$\left\{ \begin{array}{l} \frac{\partial \bar{u}_i}{\partial x_i} = 0 \\ \\ \frac{\partial \bar{u}_i}{\partial t} + \bar{u}_j \frac{\partial \bar{u}_i}{\partial x_j} = - \frac{\partial \bar{P}}{\partial x_i} + \frac{1}{Re} \frac{\partial^2 \bar{u}_i}{\partial x_j^2} - \frac{\partial \tau_{ij}^d}{\partial x_j} + F \delta_{i1} + Ri(\bar{\rho} - \bar{\rho}_b) \\ \\ \frac{\partial \bar{\rho}}{\partial t} + \bar{u}_i \frac{\partial \bar{\rho}}{\partial x_i} = \kappa \frac{\partial^2 \bar{\rho}}{\partial x_i^2} - \frac{\partial \lambda_i}{\partial x_i} \end{array} \right.$$

SGS stress

SGS density flux

SGS stress model:

$$\tau_{ij}^d \approx -2 \underbrace{(C_S \bar{\Delta})^2 | \bar{S} |}_{\nu_T} \bar{S}_{ij}$$

SGS density flux model:

$$\lambda_i \approx - \underbrace{(C_\rho \bar{\Delta})^2 | \bar{S} |}_{\kappa_T} \partial \bar{\rho} / \partial x_i$$

- Model coefficients in SGS models are computed **dynamically** as described

BUT?

The Dynamic Lagrangian SGS model (Meneveau et al., 1996)

This model tries to improve the performance of the dynamic Smagorinsky model for non-homogeneous flows.

Rationale

- Dynamic model not reliable without averaging
 - Numerical instability
- So some averaging necessary
 - Global averaging successful but requires homogeneous direction
 - Local averaging possible but results depend on volume chosen
- Need an averaging procedure that works in complex flows.

Meneveau *et al.* (1996)* developed a Lagrangian version of DSM where C_s is averaged along fluid-particle trajectories (back in time). The objective function to be minimized is given by

$$E = \int_{pathline} \epsilon_{ij}(z) \epsilon_{ij}(z) dz = \int_{-\infty} \epsilon_{ij}(z(t'), t') \epsilon_{ij}(z(t'), t') W(t - t') dt'$$

Time weighting function: $W(t - t') = T^{-1}e^{-(t-t')/T}$

$$\frac{D\mathfrak{J}_{LM}}{Dt} \equiv \frac{\partial \mathfrak{J}_{LM}}{\partial t} + \bar{u}_i \frac{\partial \mathfrak{J}_{LM}}{\partial x_i} = \frac{1}{T} (L_{ij} M_{ij} - \mathfrak{J}_{LM})$$

$$\frac{D\mathfrak{J}_{MM}}{Dt} \equiv \frac{\partial \mathfrak{J}_{MM}}{\partial t} + \bar{u}_i \frac{\partial \mathfrak{J}_{MM}}{\partial x_i} = \frac{1}{T} (M_{ij} M_{ij} - \mathfrak{J}_{MM})$$


$$(C_s \Delta)^2 = \frac{\mathfrak{J}_{LM}}{\mathfrak{J}_{MM}}$$

$$\text{Time scale } T = \theta \Delta (\mathfrak{J}_{LM} \mathfrak{J}_{MM})^{-1/8}; \quad \theta = 1.5$$

* SGS density flux computed as (Armenio and Sarkar 2002 JFM):

$$\lambda_j = -C_\rho \Delta^2 |\bar{S}| \frac{\partial \bar{\rho}}{\partial x_j} \quad C_\rho = -\frac{1}{2} \frac{\mathfrak{J}_i \mathcal{M}_i}{\mathcal{M}_k \mathcal{M}_k}$$

$$\mathcal{M}_i = \widehat{\Delta}^2 |\widehat{S}| \widehat{\frac{\partial \bar{\rho}}{\partial x_i}} - \Delta^2 \widehat{|\bar{S}|} \widehat{\frac{\partial \bar{\rho}}{\partial x_i}} \quad \mathfrak{J}_i = \widehat{\bar{\rho} \widehat{u}_i} - \widehat{\bar{\rho}} \widehat{\bar{u}_i}$$

- Lagrangian dynamic model has allowed applying the Germano identity to a number of complex-geometry engineering problem.

Examples:

LES of flow over wavy walls

Armenio & Piomelli (2000)

Flow, Turb. & Combustion.

72

V. ARMENIO AND U. PIOMELLI

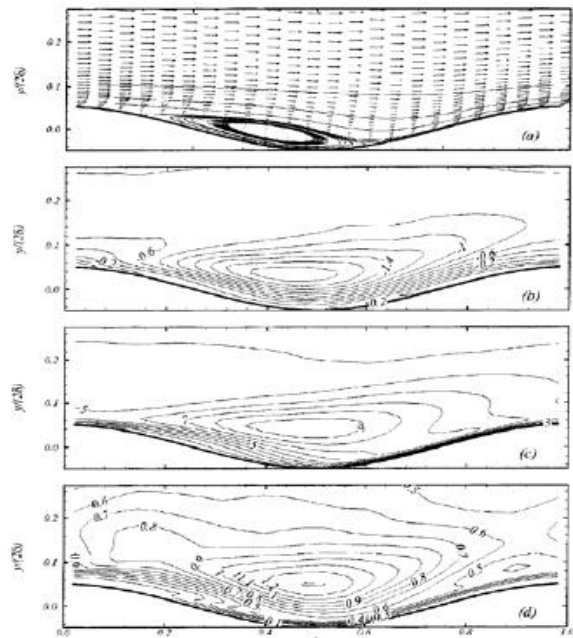
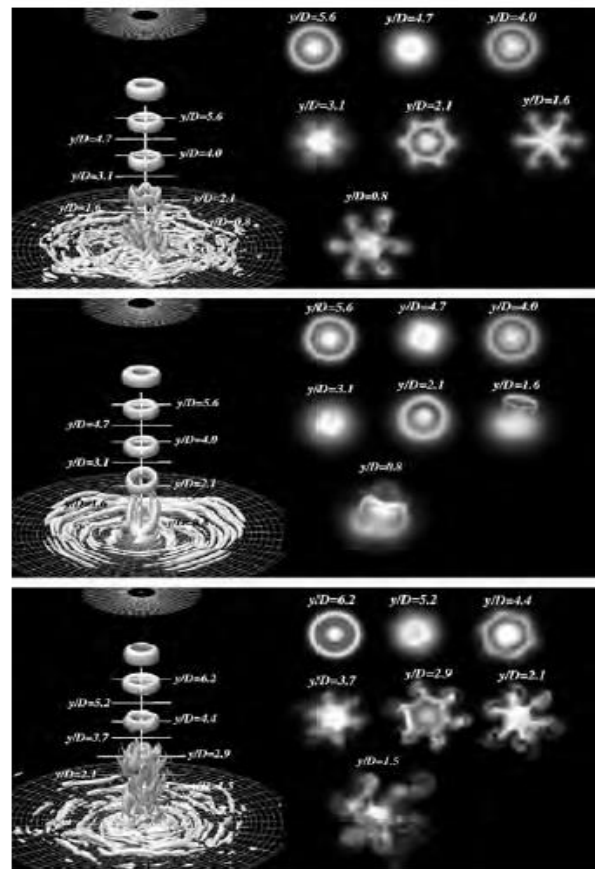


Figure 12. Wavy channel, $2a/\lambda = 0.1$; CIP simulation. (a) Mean velocity vectors and streamlines; (b) Reynolds stress ($u'v'$); (c) q^2 ; (d) normalized eddy viscosity.

4.2. LARGE-AMPLITUDE WAVE

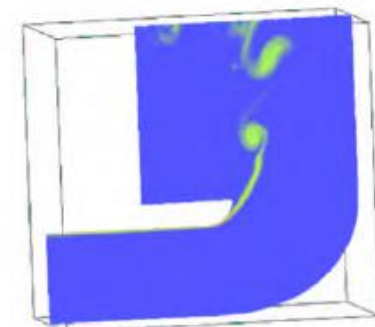
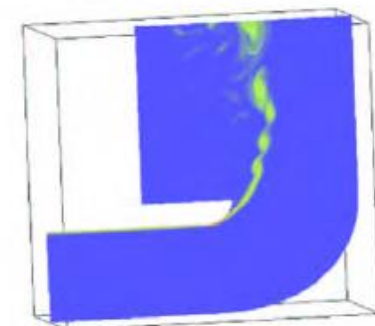
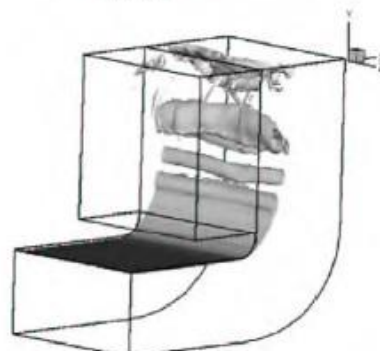
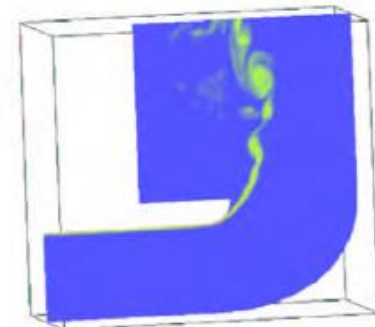
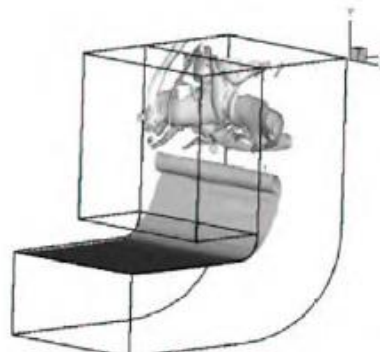
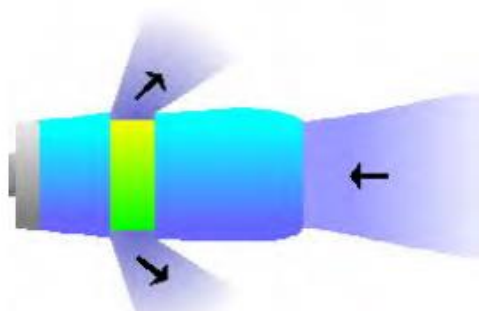
The grid and the flow parameters used for the simulation of the flow over a large-amplitude wavy wall were reported in Table III. As previously pointed out, the parameters have been chosen to fit the experiments of B93 and the LES of HS99.

LES of structure of impinging jets:
Tsubokura et al. (2003)
Int Heat Fluid Flow **24**.



Examples:

LES of flow in thrust-reversers
Blin, Hadjadi & Vervisch (2002)
J. of Turbulence.



In summary....

DNS , LES, RANS require solving the unsteady form of the NS or RANS equations.

Main differences between steady-flow and unsteady-flow solvers are:

In steady –flow algorithms, typically continuity equation is not satisfied during the time-advancement of the solution and conservation laws are fulfilled at the convergent state of the solution

In unsteady-flow solvers conservation laws are satisfied at each time step

This makes a strong difference in CPU time request.

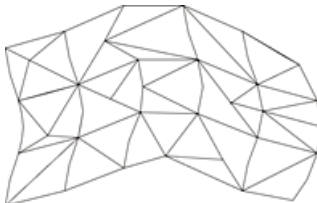
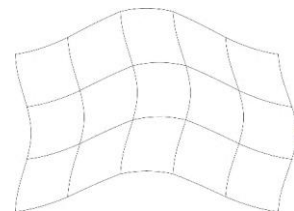
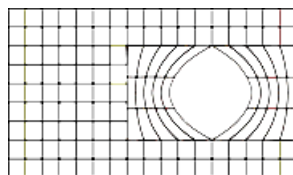
Typically projection methods are employed

Geometry

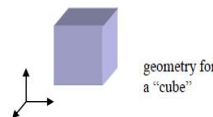
- The starting point for all problems is a “geometry.”
- The geometry describes the shape of the problem to be analyzed.
- Can consist of volumes, faces (surfaces), edges (curves) and vertices (points).
- Many different cell/element and grid types are available.
Choice depends on the problem and the solver capabilities.

Grids:

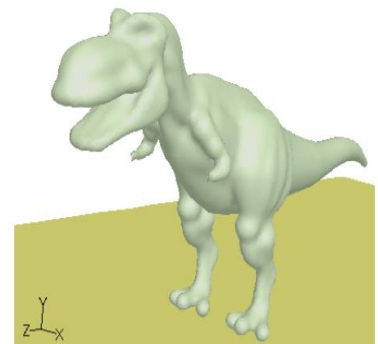
- Structured grid
 - all nodes have the same number of elements around it
 - only for simple domains
- Unstructured grid
 - for all geometries
 - irregular data structure



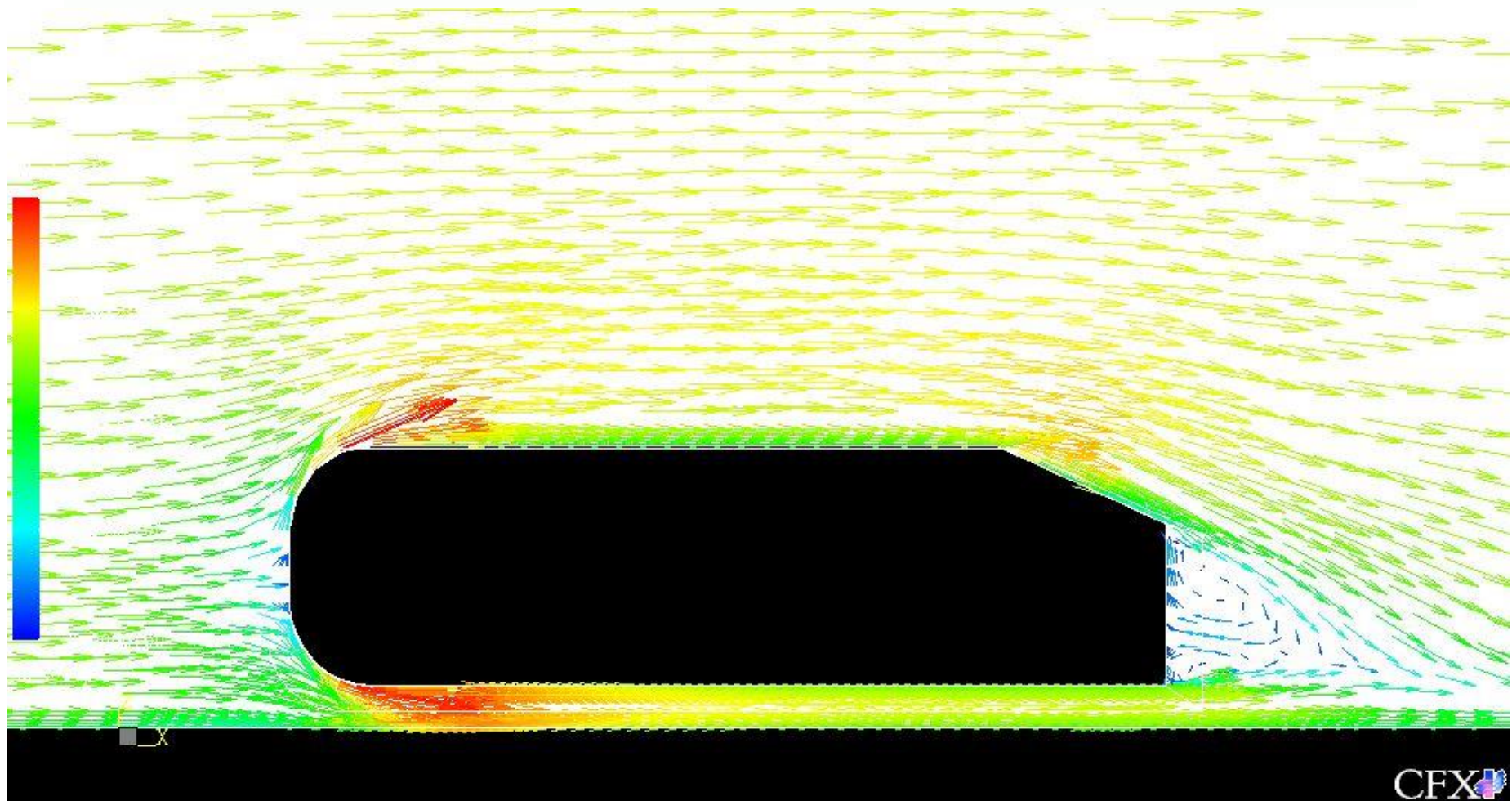
Geometry can be very simple...



... or more complex



Example



CFX

Structure/unstructured mesh

- Structured grid

Advantages:

- Economical in terms of both memory & computing time
- Easy to code/more efficient solvers available
- The user has full control in grid generation
- Easy in post processing

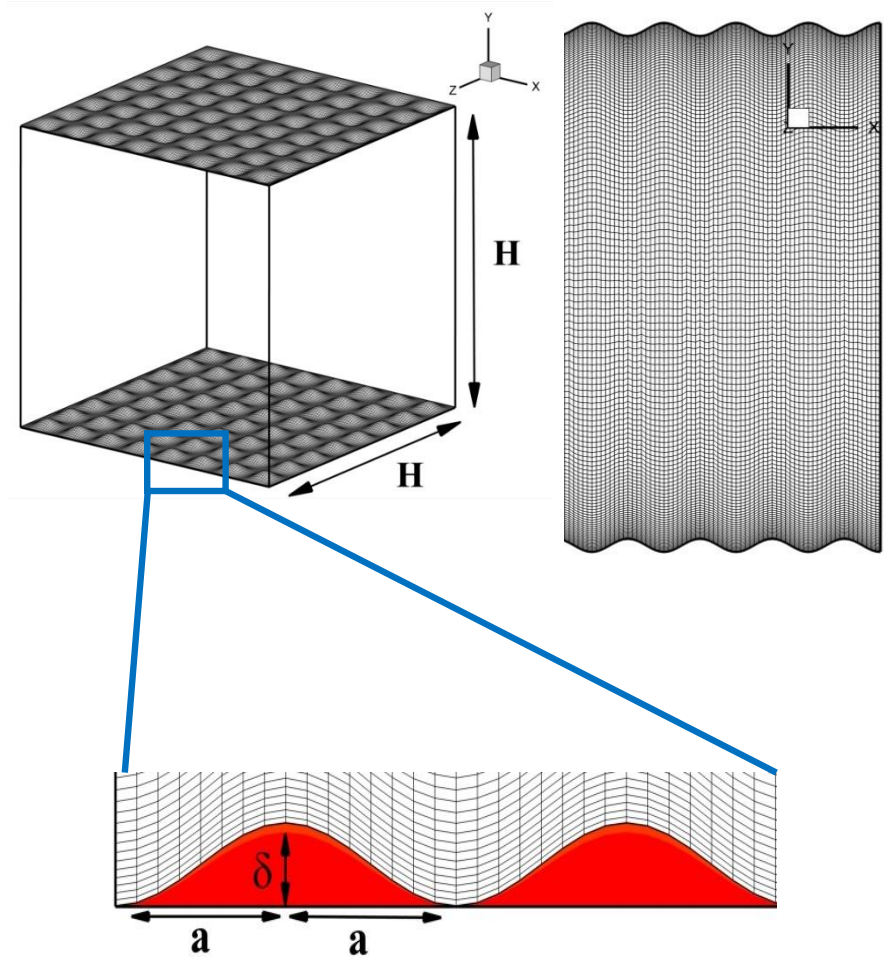
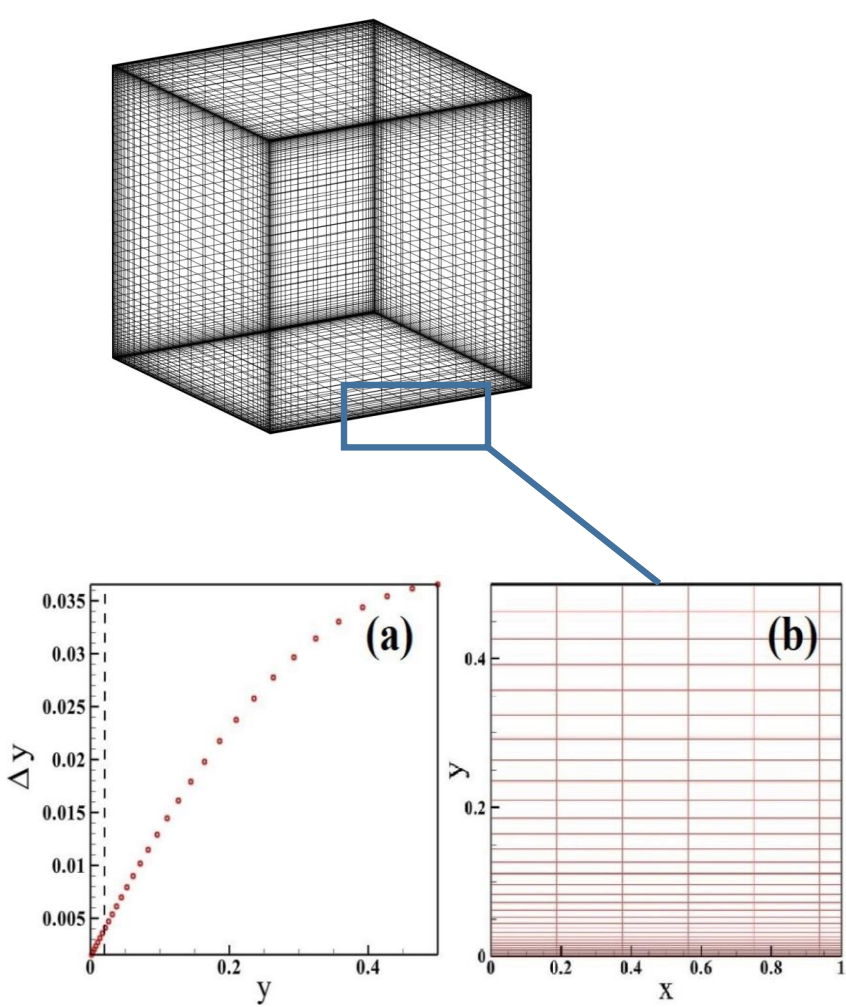
Disadvantages

- Difficult to deal with complex geometries

- Unstructured grid

- Advantages/disadvantages: opposite to above points!!

Structure/unstructured mesh

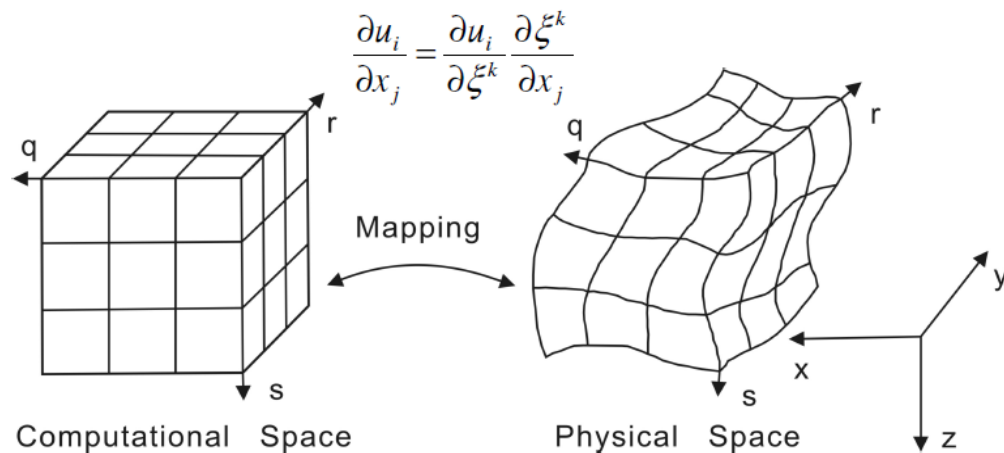


Stretched grid points within the thermal boundary layer (close to the solid wall)

Coordinates transformation

- Cartesian or curvilinear forms of the equations solved using finite difference or finite volume
- **Advantages**

Very powerful when used to reproduce simple/moderately complex geometry with non-periodic boundary conditions (inflow/outflow, solid boundaries)



Drawbacks

Exhibit good conservation features

- low-to-moderate CPU time consuming
- Suited for DNS and LES

General remarks on turbulence models

- There are no generically best models.
- Near wall treatment is generally a very important issue.
- A good mesh is important to get good accurate results.
- Different models may have different requirement on the mesh.
- Expertise/validation are of great importance to CFD.

A developed code called (AFiD) that have open source available at (www.afid.eu)

We will update our lecture note and slides soon, Insha Allah

Please don't hesitate to contact us,

nforooza@ictp.it

onime@ictp.it



The Abdus Salam
International Centre
for Theoretical Physics

Turbulent Fluid Flows in Definite Geometries and Numerical Solutions

Dr. Najmeh Foroozani

The Abdus Salam International Centre for Theoretical Physics (ICTP), Trieste Italy

Complex Fluid Flows and Its Environmental Applications

University of Lagos, Nigeria

6th – 11th June 2016

Turbulent flow

Numerical solutions

Definit geometry

Numerical study of turbulent Rayleigh-Bénard convection in a cube

Natural convection

Thermal expansion causes hot fluid to rise and cold fluid to sink.

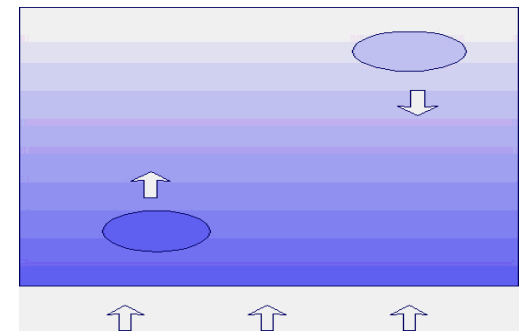
α : Fluid thermal expansion coefficient

ν : Fluid kinematic viscosity

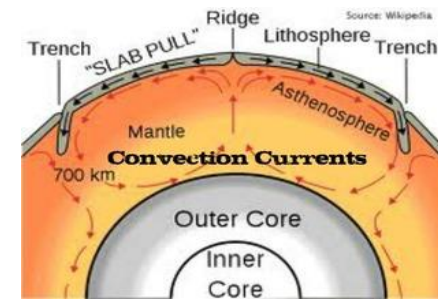
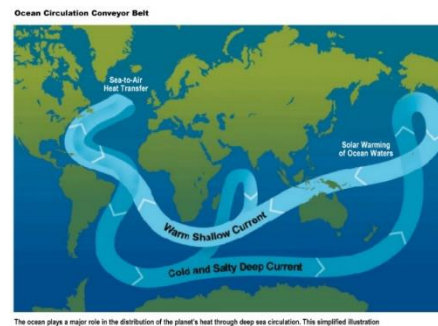
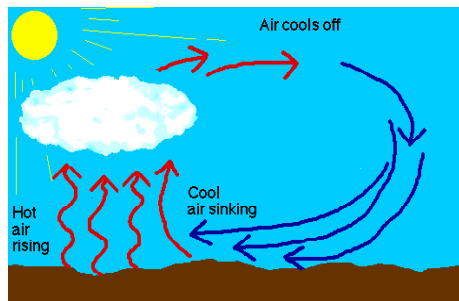
κ : Fluid thermal diffusivity

$$T \longrightarrow$$

$$T + \Delta T \longrightarrow$$

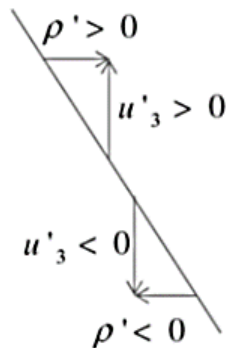


- Heat transfer mediated by a fluid takes place in countless phenomena in industrial and natural systems, for example



The vertical buoyancy flux

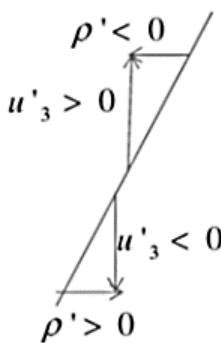
It has to be interpreted as vertical flux of mass associated to fluctuations of temperature or concentration



$$\frac{\partial \rho}{\partial z} < 0 \quad , \quad \frac{\partial T}{\partial z} > 0$$

Stable
stratified case

$$\overline{u'_3 \rho'} > 0 \quad , \quad \overline{u'_3 T'} < 0$$



$$\frac{\partial \rho}{\partial z} > 0 \quad , \quad \frac{\partial T}{\partial z} < 0$$

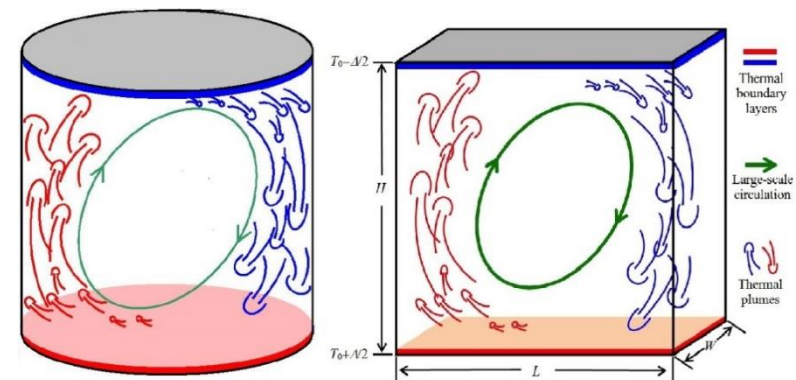
Unstable
stratified case

$$\overline{u'_3 \rho'} < 0 \quad , \quad \overline{u'_3 T'} > 0$$

The Rayleigh-Bénard problem

- Rayleigh-Bénard (RB) system: A fluid layer of depth H heated from below and/or cooled from above.
- The fluid starts moving only when $Ra > Ra_c$
(buoyancy must “exceed” viscous drag and heat diffusion)
- Control parameters for convection;

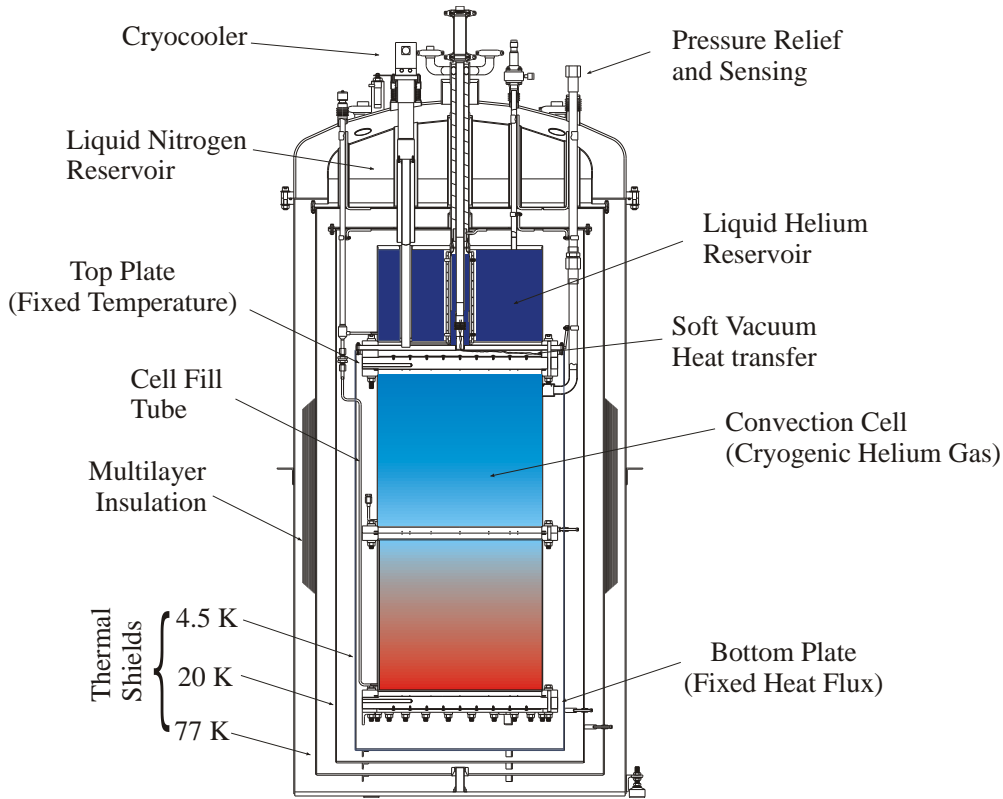
$$\begin{aligned}
 1) \quad & Ra = \frac{\alpha g \Delta T H^3}{\nu \kappa} && \text{“forcing” parameter} \\
 2) \quad & Pr = \frac{\nu}{\kappa} && \text{fluid properties} \\
 3) \quad & \Gamma = \frac{L}{H} && \text{geometry parameter}
 \end{aligned}$$



Nusselt number	$Nu = \frac{QH}{\kappa \Delta T}$
Reynold number	$Re = \frac{UH}{\nu}$

$$Ra = f(Nu, Pr, \Gamma, \text{shape})$$

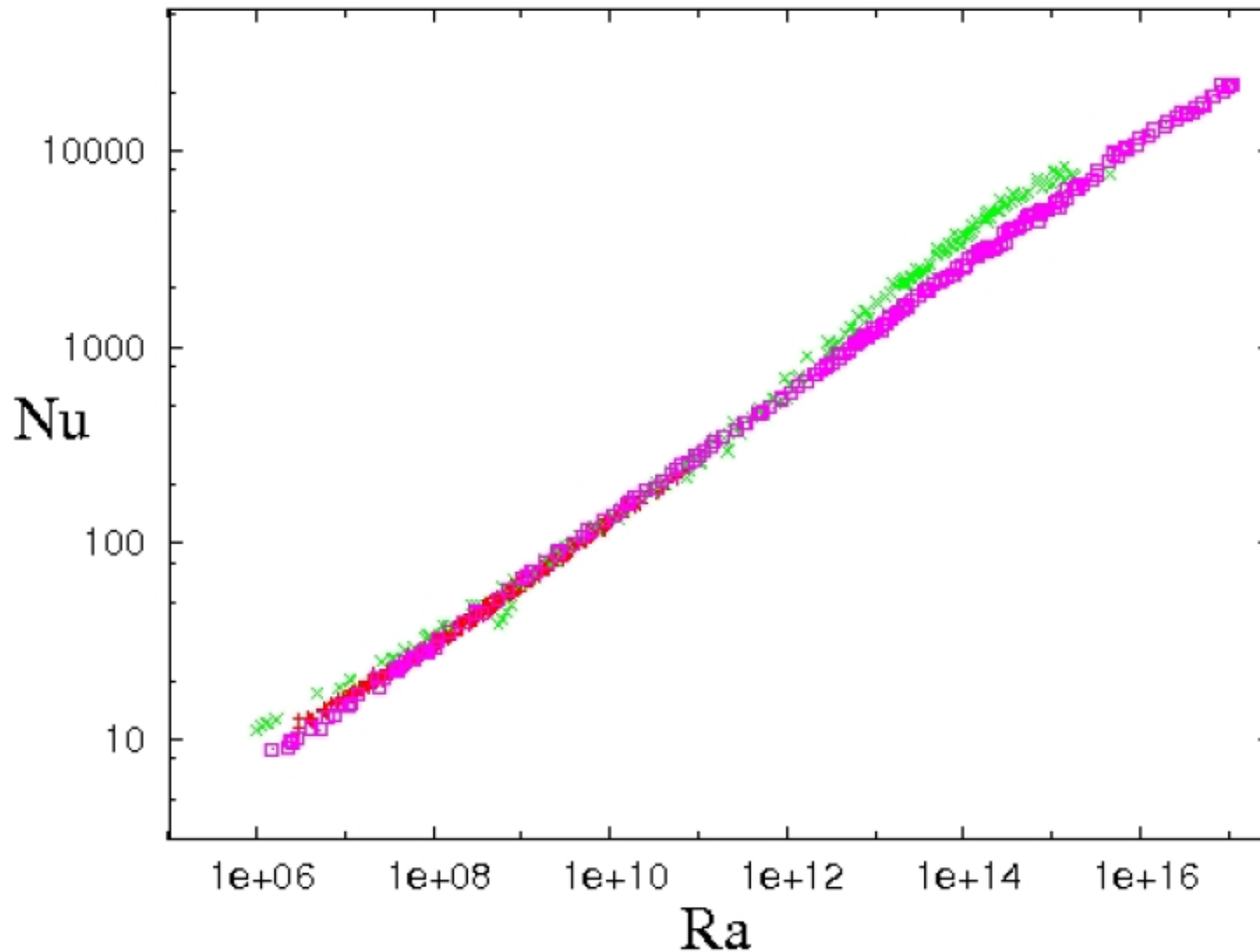
A cryogenic apparatus for very high Ra (sample height = 1 meter, diameter = 0.5 meter)



- $\text{Ra} = (\text{g}\alpha\Delta T H^3)/(\nu k) \sim \text{constant}^*(\rho^2 \alpha C_p)$. Ra increases as ρ^2 in ideal gas regime and as αC_p near critical point. αC_p is decades larger than for conventional fluids.
- 11 decades of Ra possible! Large sample height moves *entire range of Ra* into turbulent regime and indirectly extends conditions of constant Pr (ideal gas) to higher Ra .

State-of-the-Art Experiments (high Ra)

Cryogenic helium, cylindrical cell $\Gamma=1/2$



Niemela et al. (2000), Chavanne et al. (2001), Roche et al. (2002)

Motivation of the Study

VOLUME 87, NUMBER 18

PHYSICAL REVIEW LETTERS

29 OCTOBER 2001

Does Turbulent Convection Feel the Shape of the Container?

Z. A. Daya and R. E. Ecke

PHYSICAL REVIEW E 90, 063003 (2014)

Influence of container shape on scaling of turbulent fluctuations in convection

N. Foroozani,^{1,2} J. J. Niemela,¹ V. Armenio,² and K. R. Sreenivasan³

Formulation of the problem

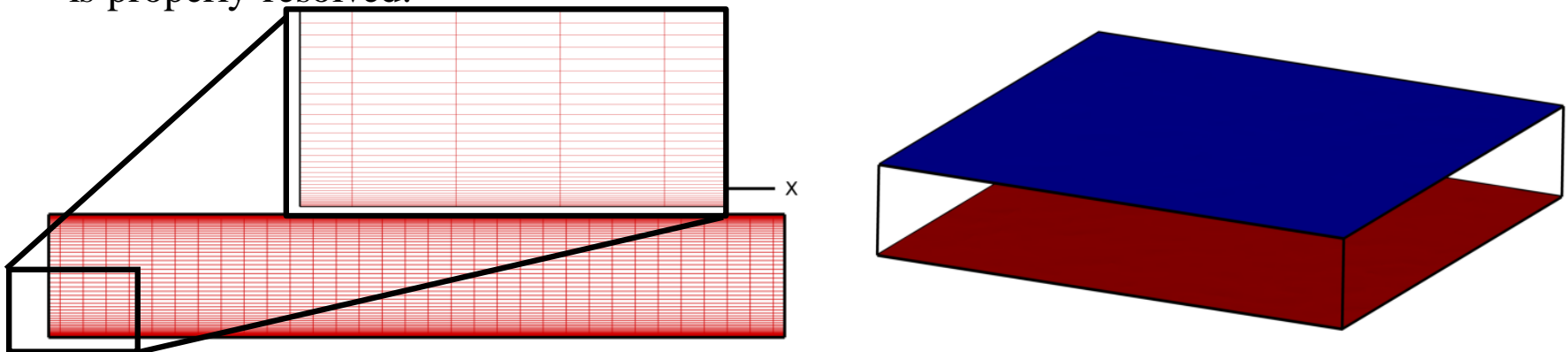
$$\frac{\partial \bar{u}_j}{\partial x_j} = 0,$$

$$\frac{\partial \bar{u}_i}{\partial t} + \frac{\partial \bar{u}_j \bar{u}_i}{\partial x_j} = -\frac{1}{\rho_0} \frac{\partial \bar{P}}{\partial x_i} + \nu \frac{\partial^2 \bar{u}_i}{\partial x_j \partial x_j} - \frac{\bar{\rho}}{\rho_0} g \delta_{i2} - \frac{\partial \tau_{ij}}{\partial x_j},$$

$$\frac{\partial \bar{\rho}}{\partial t} + \frac{\partial \bar{u}_j \bar{\rho}}{\partial x_j} = k \frac{\partial^2 \bar{\rho}}{\partial x_j \partial x_j} - \frac{\partial \lambda_j}{\partial x_j},$$

RBC with periodic walls, but why?

- First we need to find a proper numerical method in terms of definite geometry therefore we performed LES and DNS in an unbounded, homogeneous, domain.
- Our geometry is a 3D rectangular box (6,1,6) ($\Gamma = 6$), note in our study “y” is in vertical direction, with periodic boundary conditions over horizontal domain ($x-z$), no-slip velocity on the top and bottom surface, $\frac{d\rho}{\rho_0} = 1$ is applied in wall normal directions
- Molecular Prandtl number $Pr=1$ and Ra number vary $6.3 \times 10^5 \leq Ra \leq 10^8$.
- The vertical resolution in all LES was chosen such that the thermal boundary layer λ_θ is properly resolved.



The number of nodes required in thermal and viscous boundary layers computed as:

$$\begin{cases} \frac{\lambda_\theta}{H} = \frac{1}{2Nu} \\ \frac{\lambda_u}{H} \sim \frac{1}{4\sqrt{RaPr}} \end{cases}$$

$$\begin{cases} N_\theta \approx 0.35Ra^{0.15}, \quad 10^6 \leq Ra \leq 10^{10} \\ N_u \approx 0.13Ra^{0.15}, \quad 10^6 \leq Ra \leq 10^{10} \end{cases}$$

Shishkina *et al.*, 2010.

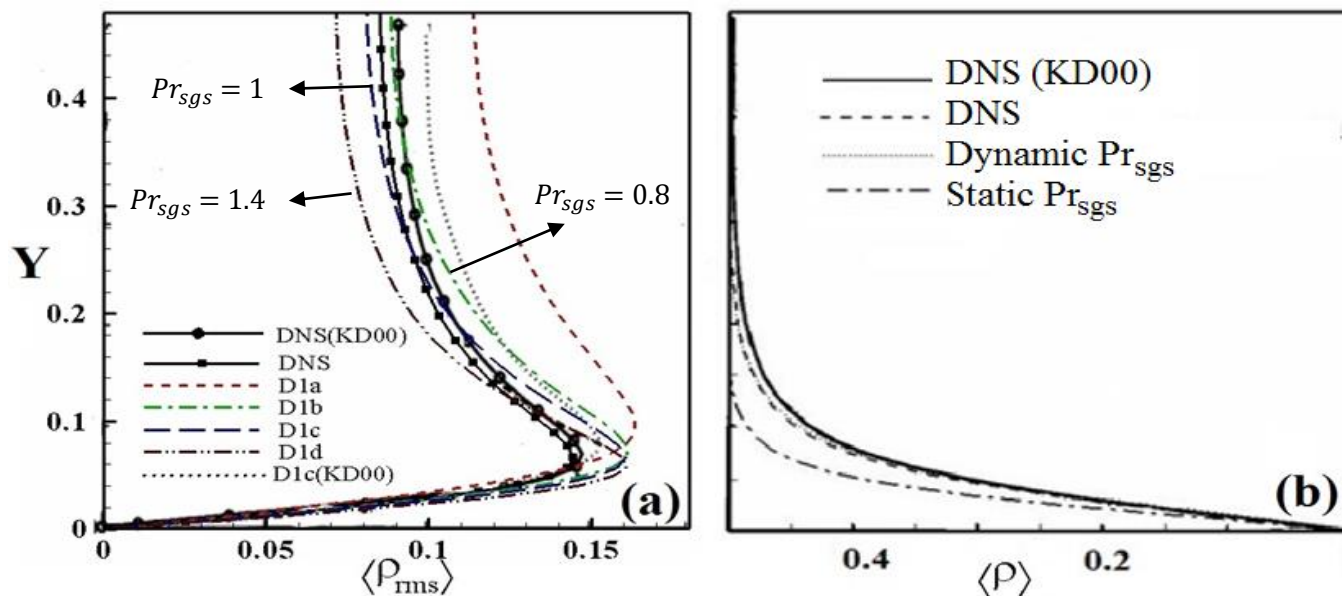
We performed two tests for LES:

- 1) $\kappa_{sgs} = \frac{v_{sgs}}{Pr_{sgs}}$ with Pr_{sgs} set *a priori* test (static)
- 2) **Both** v_{sgs} and κ_{sgs} calculated dynamically

$$\text{Total turbulent fluctuations} = \text{Resolved} + \text{SGS}$$

The resolved root-mean-square of density fluctuations computed as:

$$\rho_{rms} = [\langle \rho(x)\rho(x) \rangle_t - \langle \rho(x) \rangle_t \langle \rho(x) \rangle_t]^{1/2}$$

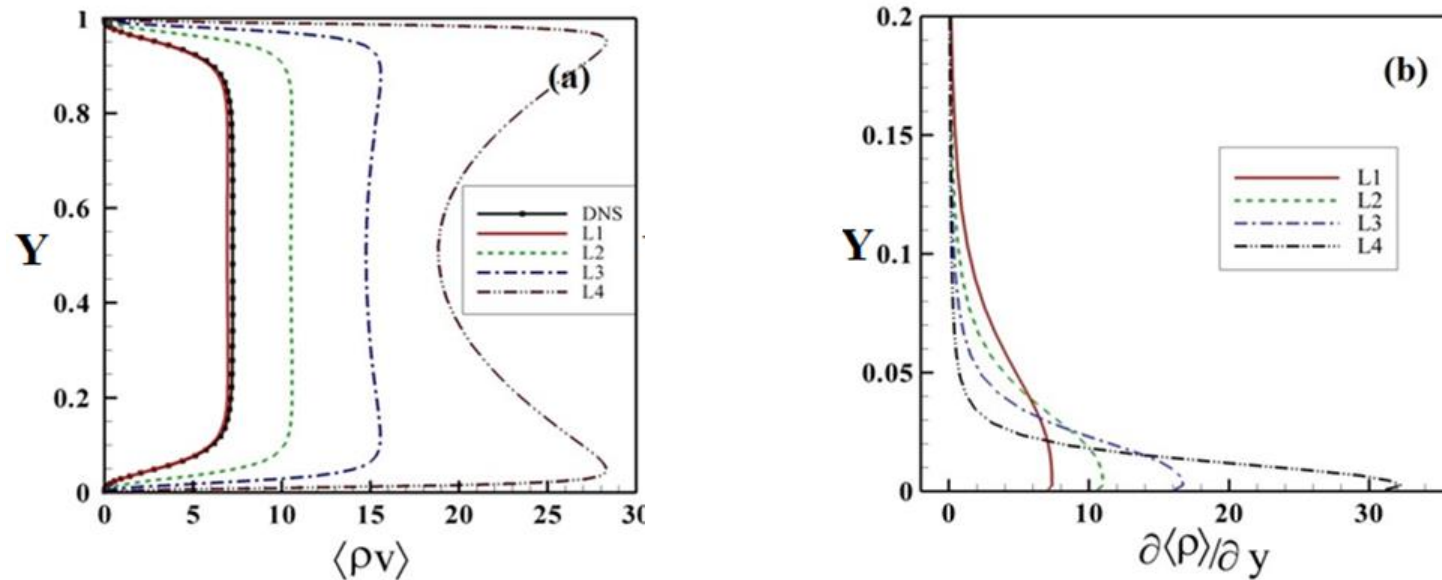


- (a) The resolved rms density fluctuations computed with the dynamic model at $\text{Ra} = 6.3 \times 10^5$ on the $32 \times 64 \times 32$ grids (b) Mean density profiles for $\text{Ra} = 6.3 \times 10^5$ with dynamic (L0) and static (D1c) Pr_{sgs} . Data are compared with Kimmel and Domaradzki (2000).

The key response of the system to the imposed parameters is the heat flux from bottom to top (Nu).

Global Nusselt number:

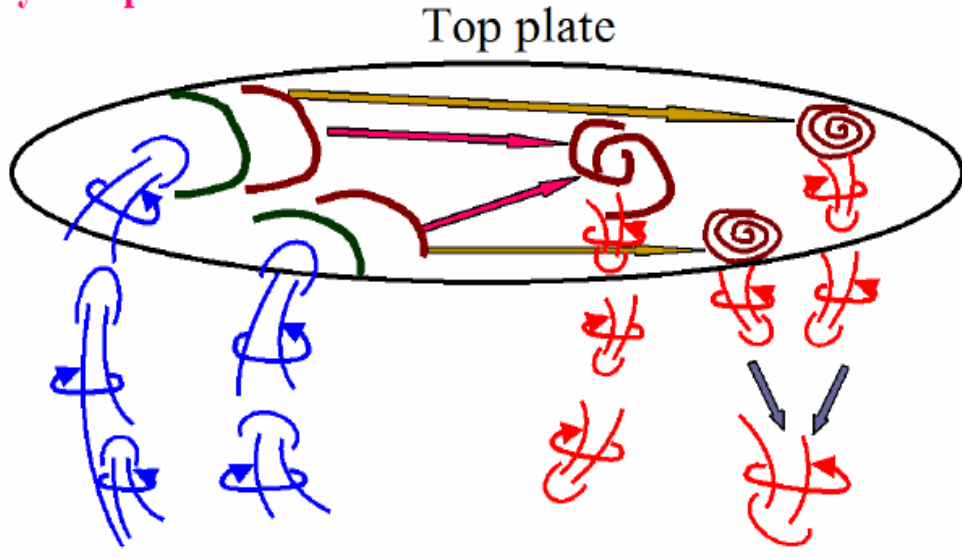
$$Nu = \frac{\langle \rho v \rangle_{A,t} - \kappa \frac{\partial \langle \rho \rangle_{A,t}}{\partial y}}{\kappa \Delta \rho / H} \rightarrow Nu = 0.14 Ra^{0.29}$$



Comparison of the Nusselt number, Nu , components using dynamic Pr_{sgs} as a function of Ra numbers; (a) resolved vertical density flux and (b) resolved density gradient along vertical direction. The letters represent $L1 (6.3 \times 10^5)$, $L2 (2.5 \times 10^6)$, $L3 (10^7)$, $L4 (10^8)$

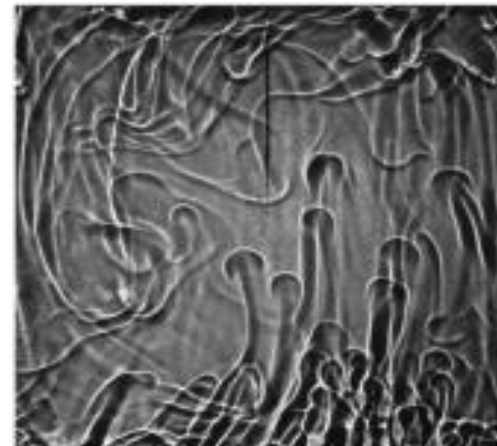
Flow topology in convection

Physical picture



- Sheetlike plume
- Convolted sheetlike plume

- Mushroomlike plume with strong vertical vorticity

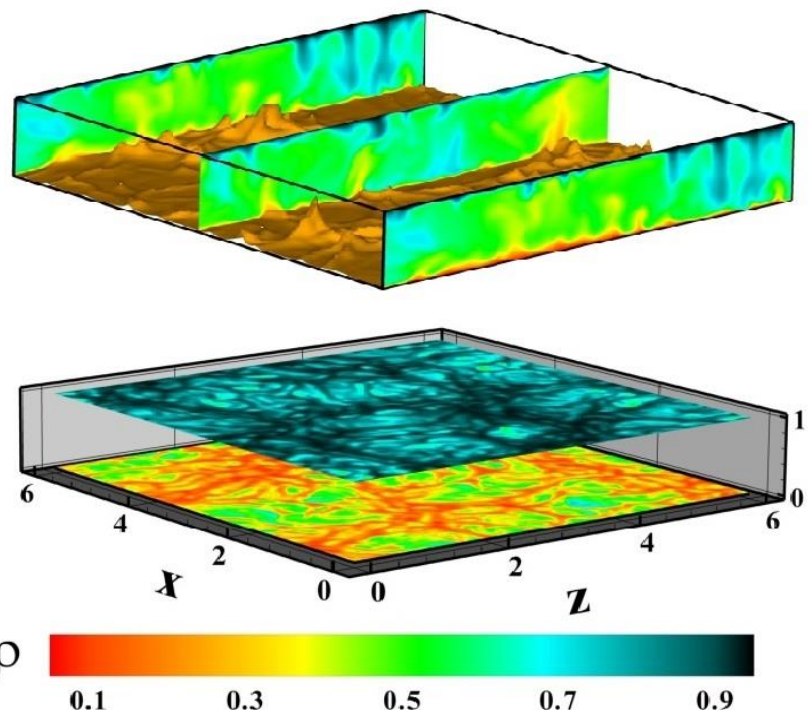


Mushroom-like plumes (side view)

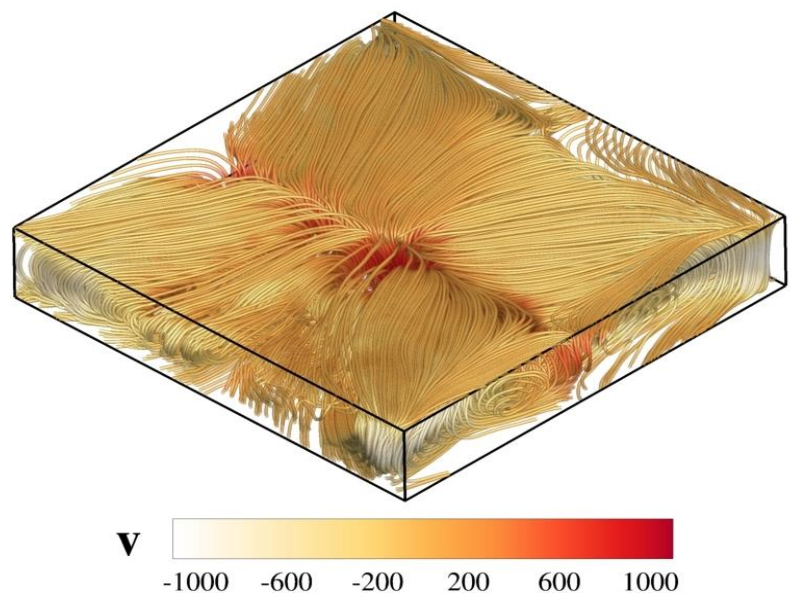
Zhang et al, PoF 2007

From simulations...

Instantaneous field



Time averaged field



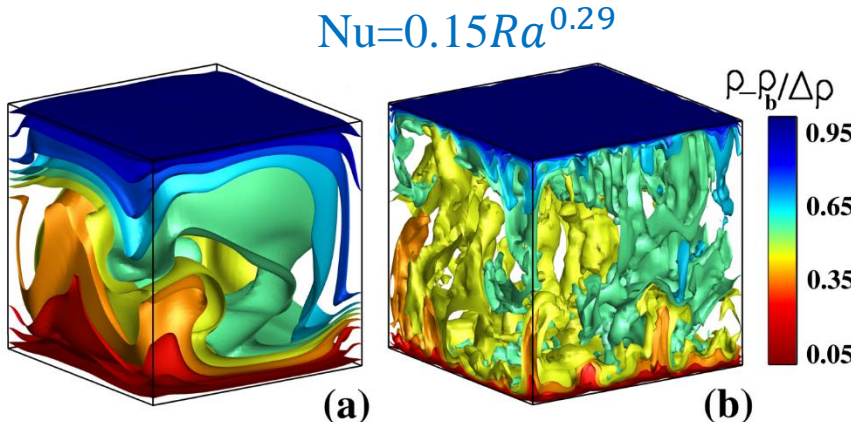
Influence of the geometry

- We perform LES in a **closed** cubic cell $\Gamma=1$, for $10^6 < Ra < 10^{10}$, molecular Prandtl number set to $Pr=0.7$
- Vertical walls are adiabatic ($\partial\rho/\partial\vec{n}=0$),
- We applied no-slip BCs at the walls,
- Finer grid close to the walls (Verzicco and Camussi JFM 2003),
- We use coarse grid at low Ra numbers, and finer resolution at high Ra. Hyperbolic tangent function is used to stretch the mesh.

- ✓ We compute global Nusselt number:

$$Nu = \frac{\kappa \partial_y \langle \rho \rangle_{A,t} - \langle u_y \rho \rangle_{A,t}}{\kappa \Delta \rho H^{-1}}$$

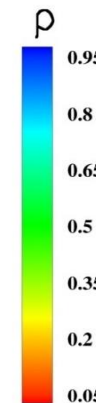
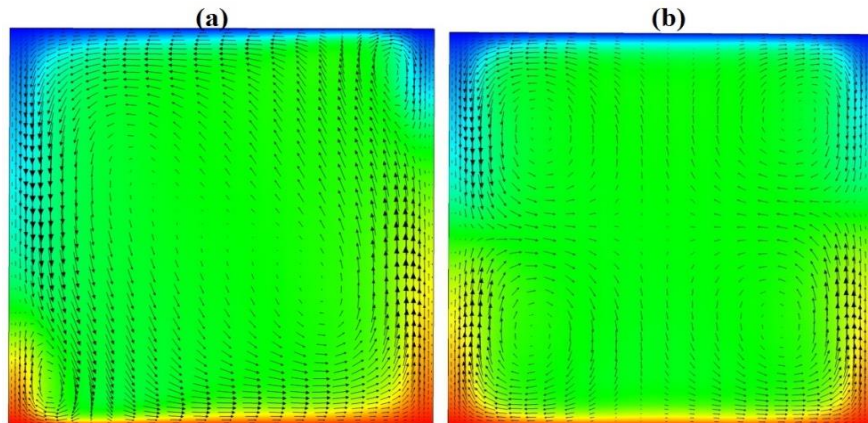
- ✓ Scaling of $Nu(Ra)$ is in good agreement with both the laboratory experiment [Qiu & Xia 1998], and DNS of Kaczorowski & Xia 2013 (JFM 722,569)



Ra	$N_x \times N_y \times N_z$	N_{BL}	Nu	Nu_{ref}
1×10^6	$32 \times 64 \times 32$	14	8.31	8.32
3×10^6	$32 \times 64 \times 32$	11	11.4	11.5
1×10^7	$32 \times 64 \times 32$	10	16.4	16.3
3×10^7	$32 \times 64 \times 32$	8	22.4	22.0
1×10^8	$32 \times 64 \times 32$	6	31.6	31.3
1×10^9	$64 \times 96 \times 64$	5	63.4	
1×10^{10}	$64 \times 96 \times 64$	5	116.2	

Structures of the mean flow

Diagonal planes



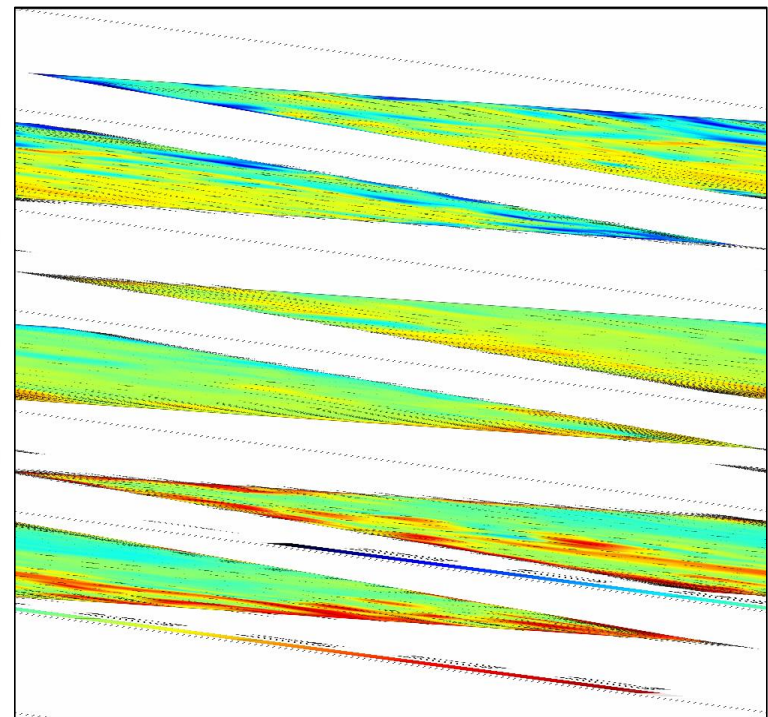
LSC is a self-organized coherent structure from thermal plumes as they propagate from the top and bottom thermal boundary layers. Orientation of the LSC is diagonal in the cube confinement.

Krishnamurti et al., 1981

Zhochi et al., 1990

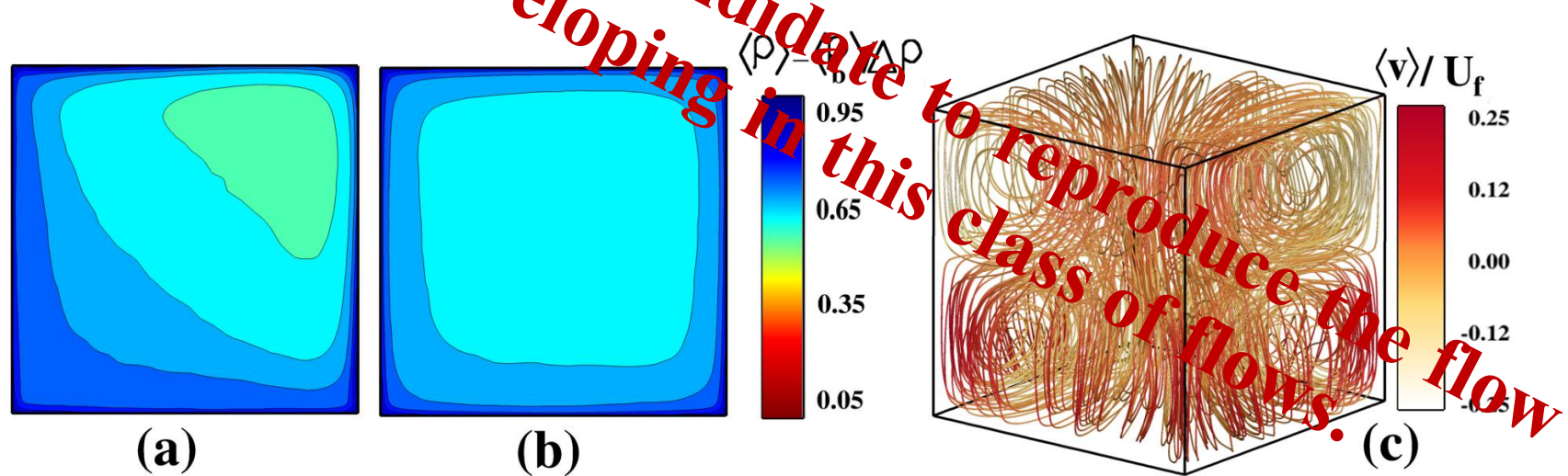
Daya & Ecke 2001

Niemela et al., 2001



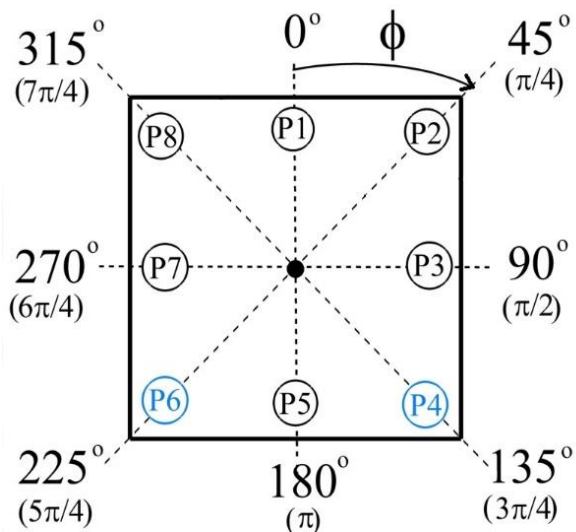
Horizontal planes near bottom
 $Y/H=0.06$, middle $Y/H=0.5$ and
top plan $Y/H=0.94$ at $Ra = 10^8$

If we average the time signal over the entire time record, in order to obtain an asymptotic Reynolds-averaging behavior, the resulting field is not representative of the flow topology. Figure (a) shows the contour plot of density close to the top boundary, obtained averaging over a time interval where the LSC is stable. It exhibits symmetry with respect to one diagonal. Long time averaging masks such ow structure (b) giving a field which is symmetric with respect to the center-line. The velocity field obtained after long-time averaging gives a symmetric eight-roll pattern not representative of the actual ow topology.

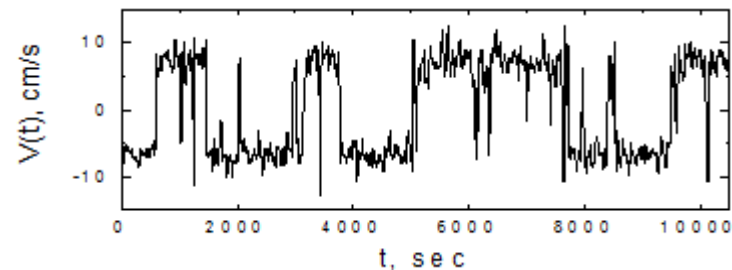


(a), (b): Contour plots of the density yield at $Y = 0.97H$ for (a) for a stable LSC pattern and (b) after long-time averaging. (c) Streamlines of the mean ow after long-time averaging showing an unrealistic 8-cell ow configuration.

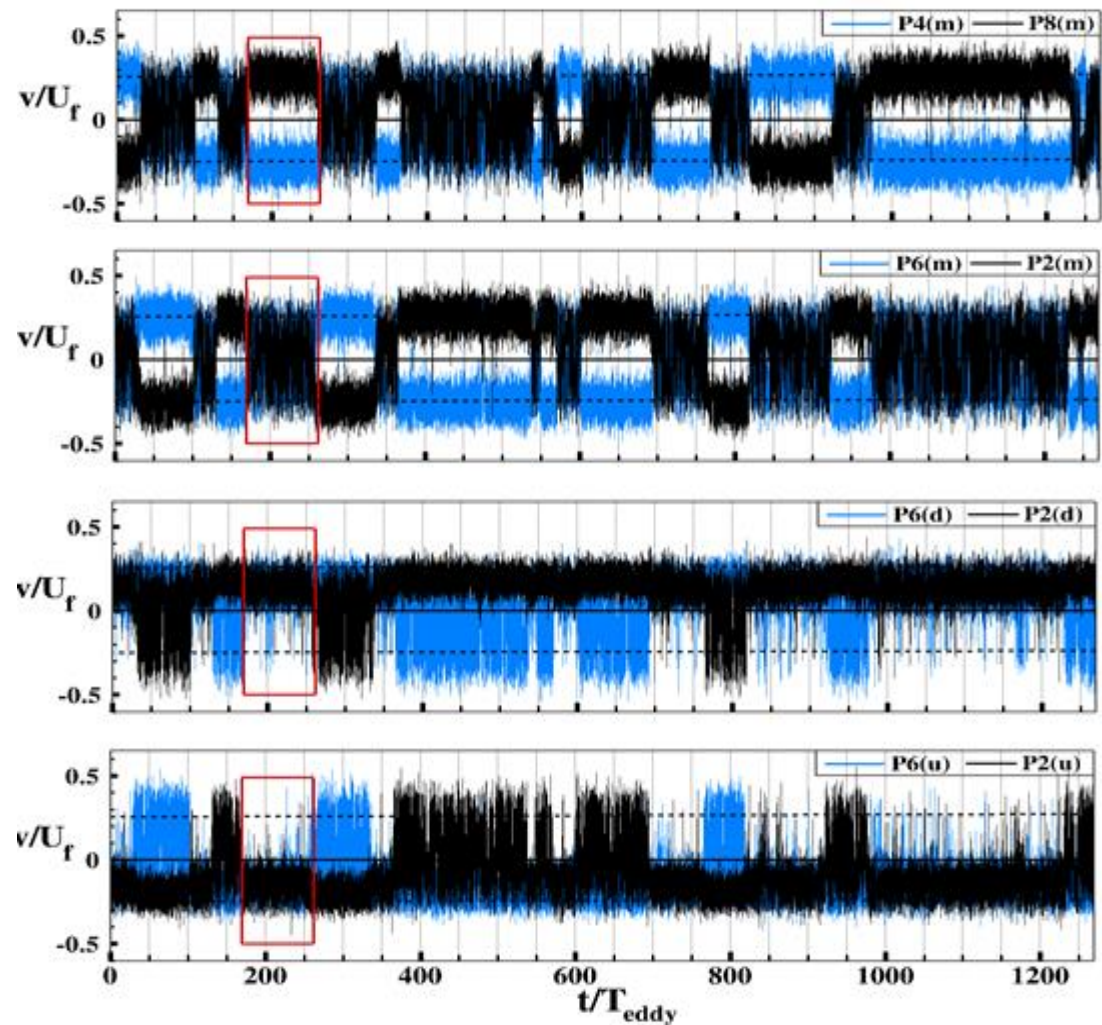
Velocity statistics



Schematic of an arbitrary horizontal plane showing the azimuthal positions for probes, placed at azimuthal angles $\varphi_i = (i\pi)/4$, $i=1,\dots,8$. The distance from the vertical walls are 0.1H for all cases.



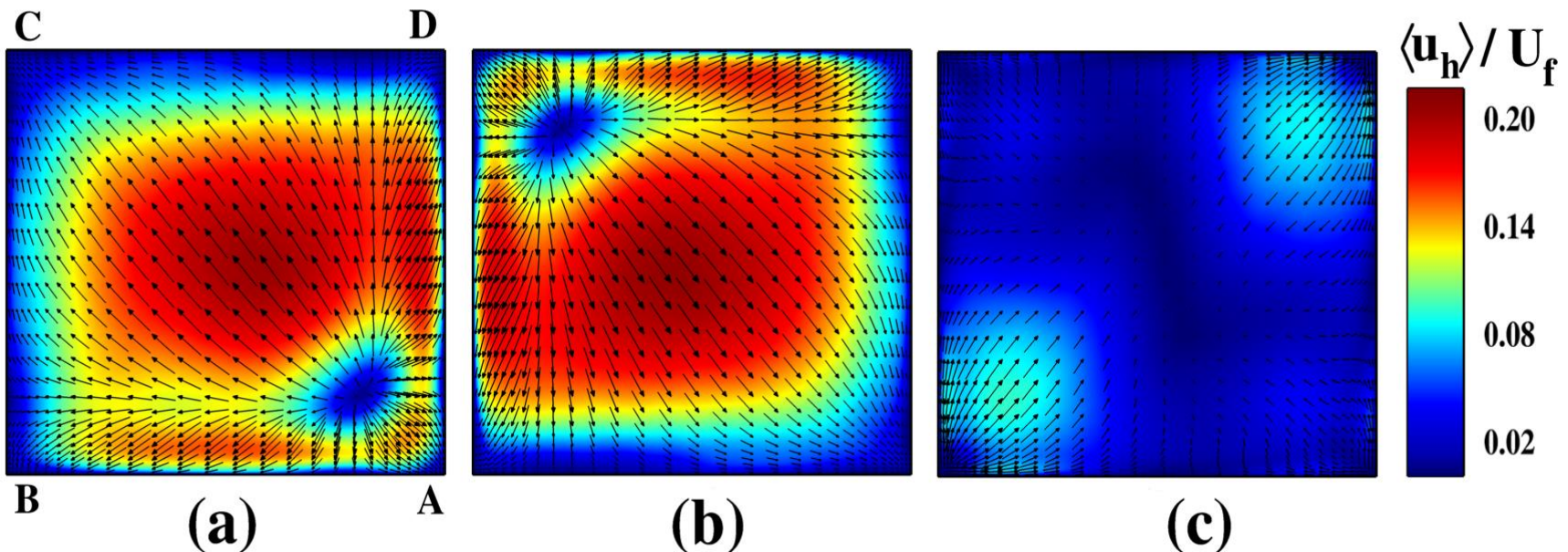
Niemela and Sreenivasan, *Nature* (2000).



Horizontal velocity near top, bottom and mid-plane

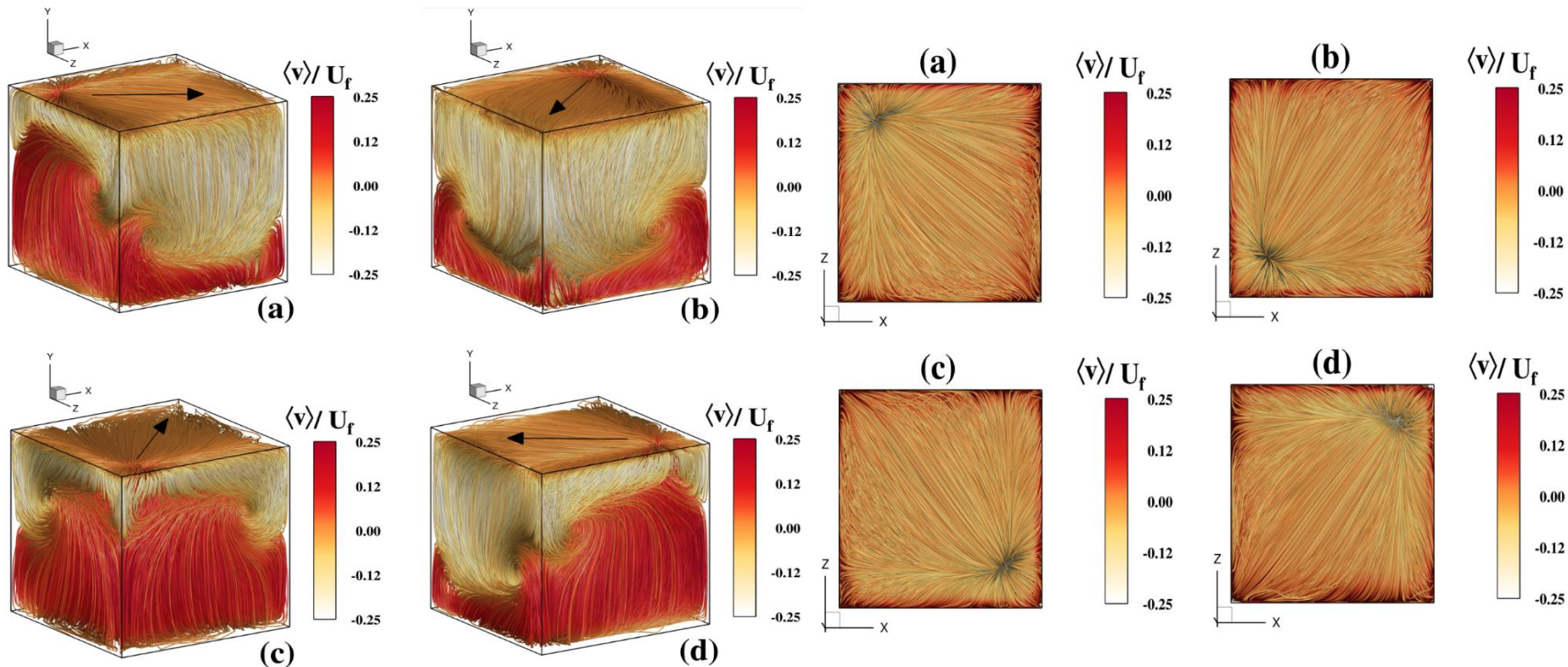
We compute horizontal velocity at different heights in cube,

$$u_h = \sqrt{U^2 + W^2}$$



3D velocity vectors superimposed on the colour-coded representation of the time-averaged, normalized horizontal velocity $\langle u_h \rangle / U_f$ at $Ra = 10^8$, $Pr = 1$, $\Gamma = 1$; (a) horizontal plane near the bottom boundary at $Y \approx 0.02H$; (b) horizontal plane near the top boundary at $Y \approx 0.98H$. and (c) horizontal plane at mid-height at $Y = 0.5H$.

Mean flow structure at $Ra = 10^8$



Time averaged of velocity streamlines. The color coding depicts the magnitude of the vertical velocity normalized by free fall velocity. The large arrow shows the direction of the LSC.

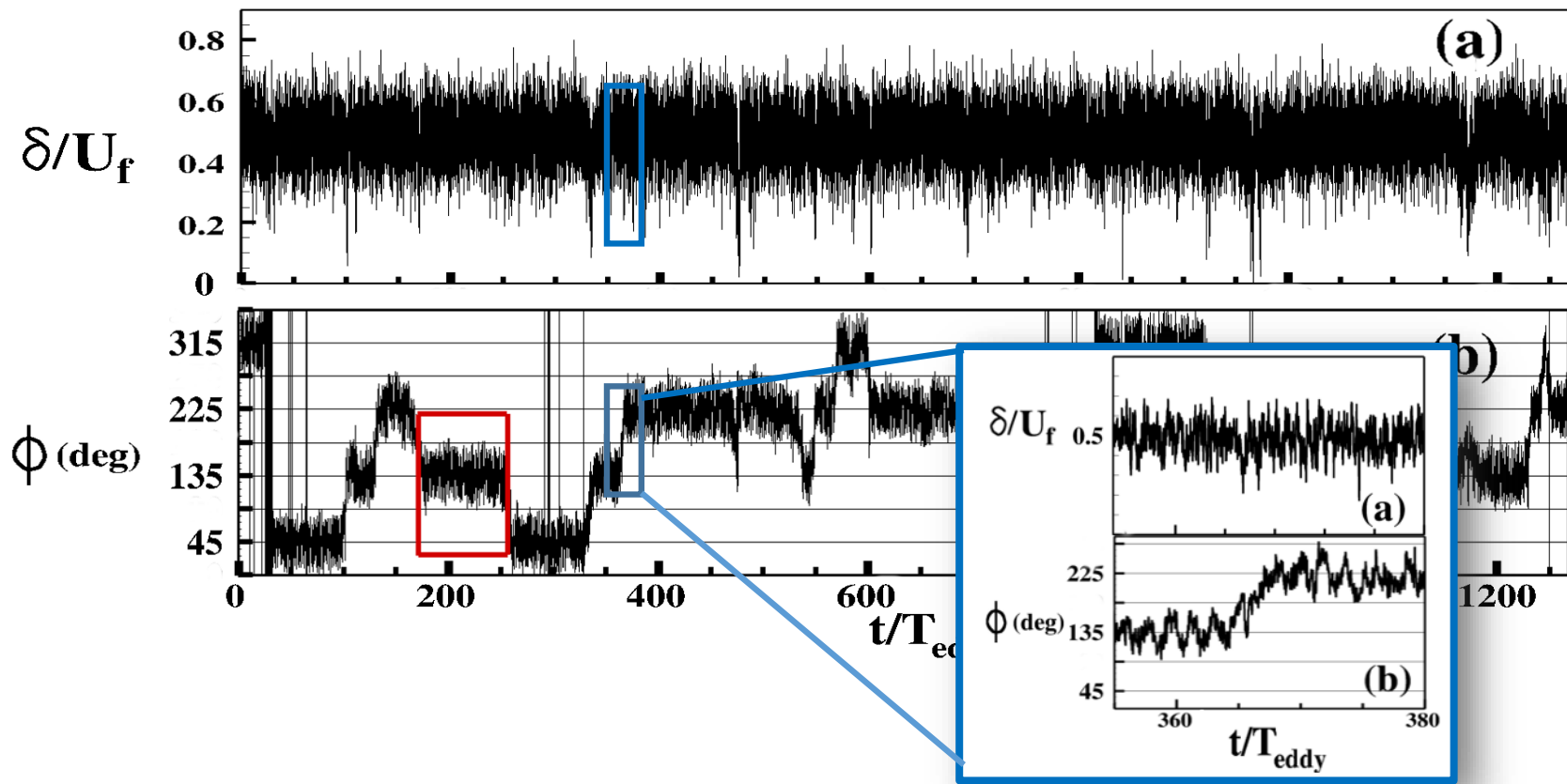
Fourier transform analysis

In order to gain a more complete understanding of the re-orientations, we compute at each time “t” the azimuthal Fourier transform of the vertical velocities $v_i(t)$ at a given probe. Thus we obtain the phase ϕ and amplitude δ of the dipole mode. The first Fourier components A_1 & B_1 are given by:

$$v_1(t) = \sum_{j=1}^8 v_j(t) \exp(-i\delta_1)$$

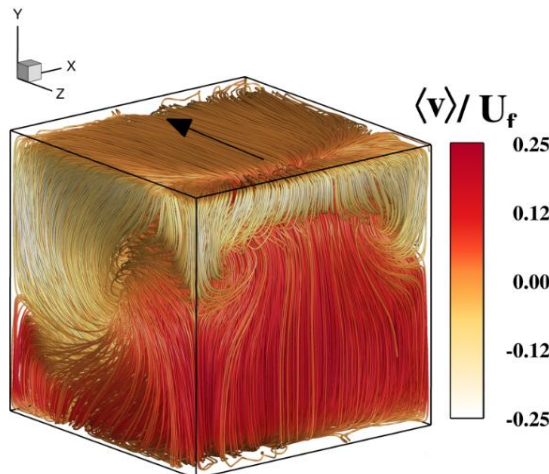
$$A_1(t) = \frac{1}{2} \sum_{j=1}^8 v_i(t) \cos \phi_i, B_1(t) = \frac{1}{2} \sum_{j=1}^8 v_i(t) \sin \phi_i$$

$$\delta(t) = \sqrt{A_1^2 + B_1^2}, \quad \phi(t) = \text{sign}(B_1) \arccos \frac{A_1}{|\delta|}.$$



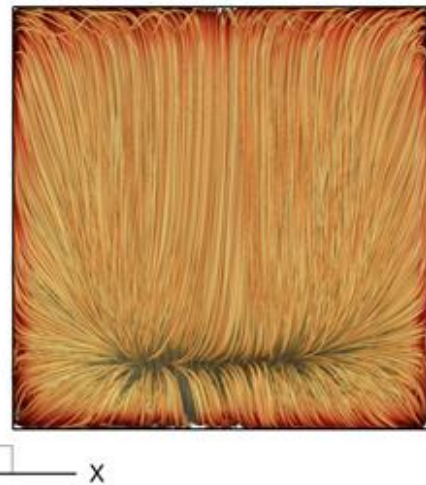
Time series of (a) the amplitude δ and (b) phase ϕ of the first Fourier mode of the vertical velocity used as an approximate measure for the reorientation of the LSC, for $Ra = 10^8$, $\text{Pr}=0.7$, $\Gamma = 1$.

Transient state during the re-orientation of the LSC

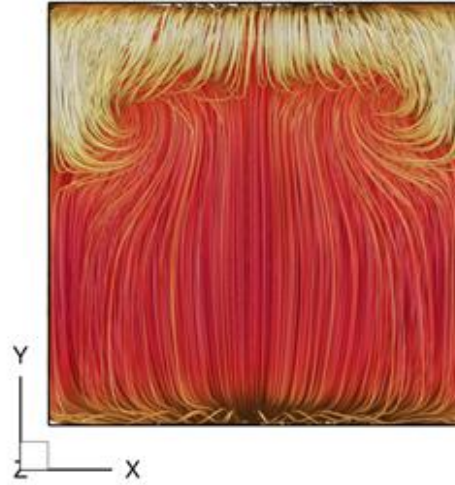


The 3D perspective of the transition state of the global flow structure during a reorientation of the LSC from one stable diagonal plane to the other.

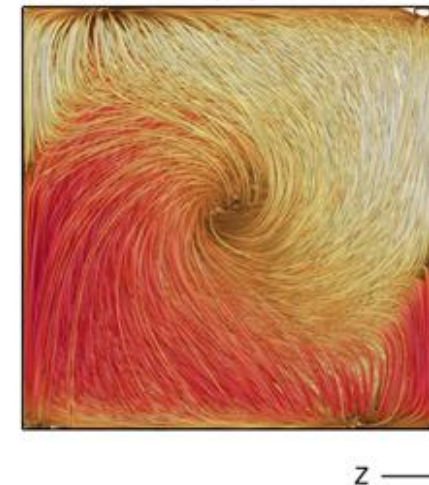
(a)



(b)



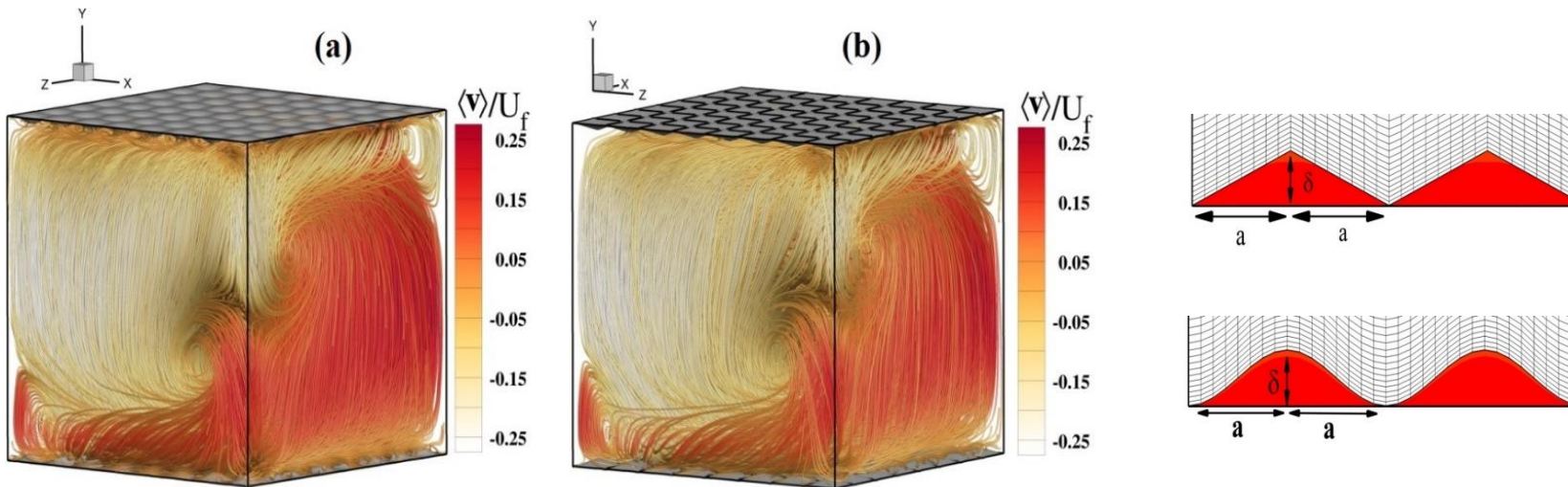
(c)



Thermal Convection in the presence of rough surfaces

- We studied* RBC with two different of roughness shapes by means of LES at $Ra = 10^8$ and $Pr = 0.7$ in a cubic cell of $\Gamma = 1$, in comparison with standard flat plate case, in order to gain better understanding of the near wall dynamics and of the 3D roughness shape effect. We desidned 3D pyramids & sinusoidal elements spread over upper and lower plates with the elements-height (δ) greater than thermal boundary layer $\delta > \lambda_\theta$.

Case	Ra	$N_x \times N_y \times N_z$	Δ_{min}/H	Δ_{max}/H	Nu
Pyramid	10^8	128^3	1.3×10^{-3}	1.3×10^{-2}	30.05
Sine-function	10^8	128^3	3.6×10^{-5}	1.3×10^{-2}	30.35



Closure

- ✓ 15 years ago numerical simulation was out of reach of computers. Nowadays computers are powerful enough to make simulations a valid alternative and a good complement to many experiments.
- ✓ The main task of turbulence modeling is to develop computational procedures of sufficient accuracy and generality for engineers to be able to accurately predict the Reynolds stresses and the scalar transport terms.
- ✓ This will then allow for the computation of the time averaged flow and scalar fields without having to calculate the actual flow fields over long time periods.

Hope you enjoyed the tour of

colorful Computational Fluid

Dynamics

Some references

1. K. R. Sreenivasan, A. Bershadskii and J. J. Niemela, Phys. Rev. E, 65, 1 (**2002**).
2. N. Foroozani, J. J. Niemela, V. Armenio and K. R. Sreenivasan, Phy. Rev. E, 90, 063003 (**2014**).
3. V. Armenio and S. Sarkar, J. Fluid Mech., 459, 1 (**2002**)
4. C. Meneveau, T. S. Lund and W. H. Cabot, J. Fluid Mech., 319, 353 (**1996**).
5. R. Ni, S. D Huang and K. Q. Xia, JFM RAPIDS., 778, R5, 1 (**2015**).
6. Daya, Ecke, Phys Rev Lett 87 184501 (**2001**).
7. E. Brown and G. Ahlers, Phys Rev Lett 98 (13) 134501, (**2007**)
8. R. Verzicco and R. Camussi, J. Fluid Mech., 477, 19 (**2003**)
9. K. Bai, D. Ji and E. Brown, arXive:1511.01081v1, Nov 3 (**2015**)